Journal of Enzyme Inhibition and Medicinal Chemistry

ISSN: 1475-6366 (Print) 1475-6374 (Online) Journal homepage: http://www.tandfonline.com/loi/ienz20

Synthesis and pharmacological evaluation of donepezil-based agents as new cholinesterase/monoamine oxidase inhibitors for the potential application against Alzheimer's disease

Fan Li, Zhi-Min Wang, Jia-Jia Wu, Jin Wang, Sai-Sai Xie, Jin-Shuai Lan, Wei Xu, Ling-Yi Kong & Xiao-Bing Wang

To cite this article: Fan Li, Zhi-Min Wang, Jia-Jia Wu, Jin Wang, Sai-Sai Xie, Jin-Shuai Lan, Wei Xu, Ling-Yi Kong & Xiao-Bing Wang (2016): Synthesis and pharmacological evaluation of donepezil-based agents as new cholinesterase/monoamine oxidase inhibitors for the potential application against Alzheimer's disease, Journal of Enzyme Inhibition and Medicinal Chemistry, DOI: 10.1080/14756366.2016.1201814

To link to this article: http://dx.doi.org/10.1080/14756366.2016.1201814

Journal of Enzyme Inhibition and Medicinal Chemistry

www.tandfonline.com/ienz
ISSN: 1475-6366 (print), 1475-6374 (electronic)

J Enzyme Inhib Med Chem, Early Online: 1–13
 DOI: 10.1080/14756366.2016.1201814

Taylor & Francis
Taylor & Francis Group

RESEARCH ARTICLE

Synthesis and pharmacological evaluation of donepezil-based agents as new cholinesterase/monoamine oxidase inhibitors for the potential application against Alzheimer's disease

Fan Li, Zhi-Min Wang, Jia-Jia Wu, Jin Wang, Sai-Sai Xie, Jin-Shuai Lan, Wei Xu, Ling-Yi Kong, and Xiao-Bing Wang

State Key Laboratory of Natural Medicines, Department of Natural Medicinal Chemistry, China Pharmaceutical University, People's Republic of China

Abstract

In a continuing effort to develop multitargeted compounds as potential treatment agents against Alzheimer's disease (AD), a series of donepezil-like compounds were designed, synthesized and evaluated. *In vitro* studies showed that most of the designed compounds displayed potent inhibitory activities toward AChE, BuChE, MAO-B and MAO-A. Among them, **w18** was a promising agent with balanced activities, which exhibited a moderate cholinesterase inhibition (IC_{50}, 0.220 μM for eeAChE; 1.23 μM for eqBuChE; 0.454 μM for hAChE) and an acceptable inhibitory activity against monoamine oxidases (IC_{50}, 3.14 μM for MAO-B; 13.4 μM for MAO-A). Moreover, **w18** could also be a metal-chelator, and able to cross the blood–brain barrier with low cell toxicity on PC12 cells. Taken together, these results suggested that **w18** might be a promising multitargeted compound for AD treatment.

Keywords

Alzheimer's disease, donepezil, cholinesterase, monoamine oxidase, molecular modeling

History

Received 25 April 2016
Revised 2 June 2016
Accepted 4 June 2016
Published online 6 July 2016

Introduction

Alzheimer's disease (AD), the most common cause of dementia in elderly people, is a complex and progressive neurodegenerative disorder characterized by memory loss, decline in language ability and other cognitive imparment[1,2]. Over 100 years, the exact etiology of AD still remain elusive, multiple factors such as β-amyloid deposite, dyshomeostasis of biometal, oxidative and low levels of acetylcholine (ACh) are considered to play significant roles in the pathophysiology of AD[3].

Among the multiple factors that induce AD, the cholinergic hypothesis has been proposed to explain the mechanism of AD development[4]. This hypothesis asserts that dysfunction of cholinergic system, mainly decline of acetylcholine (ACh) level, leads to the memory and cognitive deficits associated with AD, and inhibiting the cholinesterase (ChE) responsible for the hydrolysis of ACh is therefore supposed to be clinically beneficial to patients[5,6]. Two types of ChEs, acetycholinesterase (AChE) and butyrylcholinesterase (BuChE), existed in the central nervous system of human. Compared to BuChE, AChE is more active and can hydrolyze the major ACh in healthy brains[7]. However, in the case of AD, BuChE is a major modulator in regulating the ACh level[8,9]. As AD progresses, the activity of AChE is found to be decreased, and that of BuChE is significantly increased in the hippocampus and temporal cortex[10,11]. Consequently, both AChE and BuChE are important target, and inhibition of both of them will be more beneficial to the treatment of AD.

In addition, many studies have found that monoamine oxidase (MAO) also play a very important role in the pathogenesis of AD, as the increase of MAO in brain may result in a cascade of biochemical events leading to neuronal dysfunction[12,13]. MAOs are important FAD-dependent enzymes (flavoenzymes), which have two functional isozymic forms, namely MAO-A and MAO-B, identified by their different substrate and inhibitor specificity[14,15]. Catecholaminergic neurons predominantly contain MAO-A, while MAO-B is located in serotonergic glia and neurons[16,17]. The MAOs have been used as drug targets and inhibitors of these enzymes are used to treat neuropsychiatric syndromes[18,19]. Selective MAO-B inhibitors have been applied to treat the neurodegenerative disorders such as Alzheimer's and Parkinson's diseases[18], while selective MAO-A inhibitors have been revealed to treat depression and anxiety[19]. Several lines of evidence indicate that, AD patients also commonly present depressive symptom[20]. Based on these aspects, simultaneous inhibition of both MAO-A and MAO-B, could provide additional benefits in AD therapy.

At present, there are three FDA-approved drugs for AD treatment, these anti-AChE agents include galanthamine, donepezil, and rivastigmine, which can only provide a temporary symptom alleviation instead of preventing or slowing the progressive neurodegeneration[21–23]. However, the multiple etiologies of AD make single-target strategy difficult to shed good therapeutic effect. Thus, multi-target-directed ligand (MTDL) raises as an effective strategy for the treatment of AD[24,25]. Attempts to combine anti-AChE and anti-MAO activities in one

Address for correspondence: Ling-Yi Kong and Xiao-Bing Wang, State Key Laboratory of Natural Medicines, Department of Natural Medicinal Chemistry, China Pharmaceutical University, 24 Tong Jia Xiang, Nanjing 210009, People's Republic of China. Tel/Fax: +86-25-83271405. E-mail: cpu_lykong@126.com; xbwang@cpu.edu.cn

molecular entity have previously been reported[26]. For example, *N*-pyrimidine-4-acetylaniline derivatives possessing AChE and reversible MAO-A inhibitory activity *in vitro* have been reported, and our group has also reported the synthesis of tacrine–coumarin hybrids as multitargeted agents against AD[27–29].

Recently, donepezil, an effective anti-AChE drug for AD treatment, has attracted considerable attention[30,31]. Replacing the indanone fragment of donepezil with additional bioactive molecules to produce multitargeted inhibitors is a good strategy. For example, donepezil and *N*-[(5-(benzyloxy)-1-methyl-1*H*-indol-2-yl)methyl]-*N*-methylprop-2-yn-1-amine hybrids have been designed as multitargeted agents capable of inhibiting ChEs and MAOs[32]. On the other hand, lazabemide and its analog Ro 16–6491 are reversible MAO inhibitors with remarkably high potency and selectivity for MAO-B[33,34]. They could serve as adjuvants in the therapy of AD and other degenerative brain disorders[35]. Moreover, moclobemide, a another reversible and short-acting preferential MAO-A inhibitor, and it has been shown to have antidepressant effects on human[36,37]. The neurochemical and pharmacological characteristics of these carboxamide derivatives lazabemide, Ro16–6491 and moclobemide have been studied as to effect monoamine levels in human brain[33–37].

Given the activities of them, and in an attempt to obtain new multi-targeted molecules with both ChEs and MAOs inhibitory activity for the treatment of AD[38,39], a series of novel compounds have been designed and synthesized. The strategy is to retain the 1-benzylpiperidine fragment from donepezil with ChEs inhibition and introduce the benzamide or 2-picolinamide moiety from lazabemide, Ro16–6491 and moclobemide with MAOs inhibitory activity (Figure 1). Besides, we also introduces a 2-thiophenecarboxamide moiety for its structural similarity to benzamide. Since the length of the linker could affect the accommodation of the hybrid in AChE[40], we changed the length of carbon spacer to obtain optional conformation that could make the activity of designed compounds better. Although a part of donepezil-like compounds have been known, their biological activities such as the inhibition of ChEs and MAOs have not been determined[41–43]. Meanwhile, the amide of 2-picolinamide moiety also has the ability to chelate metal ions[44,45]. In this study, we described the design, synthesis, and evaluation of series of donepezil-like compounds which were found to show potential abilities, including the inhibition of ChEs, inhibition of MAOs, metal chelation and penetration of the blood–brain barrier (BBB). The structure–activity relationships were discussed based on the pharmacological activities. Moreover, to further investigate the interaction mechanism with ChEs and MAOs, kinetic analysis and molecular modeling studies were also performed.

Materials and methods

Materials

All common reagents and solvents were obtained from commercial suppliers and used without purification. Reaction progress was monitored using analytical thin layer chromatography (TLC) on precoated silica gel GF254 plates (Qingdao Haiyang Chemical Plant, Qing-Dao, China), and the spots were detected under UV light (254 nm). Melting points were determined on an XT-4 micromelting point instrument and uncorrected. IR (KBr-disc) spectra were recorded by Bruker Tensor 27 spectrometer (Bruker, Karlsruhe, Germany). Column chromatography was performed on silica gel (90–150 μm; Qingdao Marine Chemical Inc.). ^{1}H NMR and ^{13}C NMR spectra were measured on a Bruker ACF-500 spectrometer (Bruker, Karlsruhe, Germany) at 25 °C and referenced to TMS. Chemical shifts are reported in ppm (δ) using the residual solvent line as internal standard. Mass spectra were obtained on a MS Agilent 1100 (Agilent Technologies, Santa Clara, CA) Series LC/MSD Trap mass spectrometer (ESI-MS) and a Mariner ESI-TOF spectrometer (HRESIMS), respectively.

General procedures for the preparation of compounds ***w1–23***

A solution of **1a–u** (1.0 mmol) and 1, 0-carbonyldiimidazole (1.2 mmol) in 10 mL of anhydrous CH_2Cl_2 was stirred at room temperature for 1 h. The 1-benzylpiperidin-4-amine or 2-(1-benzylpiperidin-4-yl) ethanamine (1.0 mmol) was added to the solution, and stirring was continued overnight. The reaction mixture was diluted with H_2O and extracted with CH_2Cl_2. The organic extracts were combined, washed with brine, and dried with anhydrous Na_2SO_4, and the solvent was evaporated *in vacuo* to give the crude product, which was purified by silica gel chromatography with CH_2Cl_2:MeOH = 30:1 as an eluent to afford corresponding target compounds.

*N-(1-benzylpiperidin-4-yl)benzamide (**w1**).* Yield 68%, white solid, m.p. 171–173 °C; IR (KBr) ν 3303, 2916, 2792, 1632,

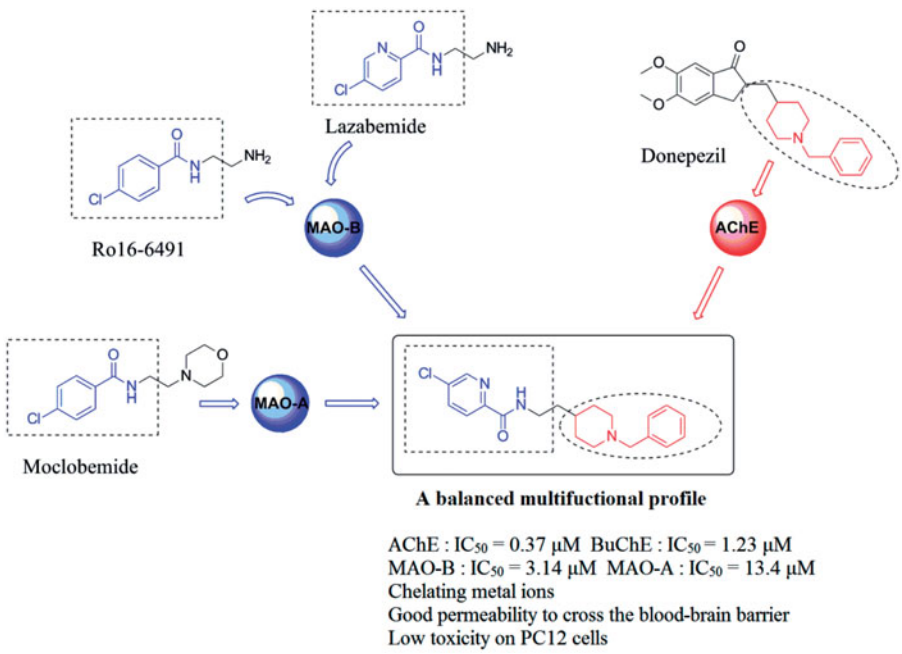

Figure 1. Design strategy for donepezil-like compounds.

1548, 1381, 1341, 743, 701 cm^{-1}; ^1H NMR (500 MHz, DMSO) δ 8.24 (d, $J = 7.7$ Hz, 1H), 7.85 (d, $J = 7.2$ Hz, 2H), 7.53 (t, $J = 7.2$ Hz, 1H), 7.46 (t, $J = 7.4$ Hz, 2H), 7.37–7.30 (m, 4H), 7.29–7.25 (m, 1H), 3.85–3.71 (m, 1H), 3.48 (s, 2H), 2.84 (d, $J = 11.0$ Hz, 2H), 2.04 (t, $J = 11.0$ Hz, 2H), 1.79 (d, $J = 10.6$ Hz, 2H), 1.60 (qd, $J = 12.1$, 3.5 Hz, 2H). ^{13}C NMR (125 MHz, DMSO) δ 166.21, 138.96, 135.22, 131.48, 129.26, 128.63, 127.72, 127.36, 62.58, 52.70, 47.39, 31.89. ESI-MS *m/z*: 295.12 $[M + H]^+$; HRMS: calcd for $C_{19}H_{22}N_2O$ $[M + H]^+$ 295.1805, found 295.1803.

*N-(1-benzylpiperidin-4-yl)-4-chlorobenzamide (**w2**).* Yield 73%, pale white solid, m.p. 192–194 °C; IR (KBr) ν 3340, 2924, 1631, 1544, 1453, 1070, 803, 757, 706 cm^{-1}; ^1H NMR (500 MHz, DMSO) δ 8.32 (d, $J = 7.6$ Hz, 1H), 7.88 (d, $J = 8.1$ Hz, 2H), 7.54 (d, $J = 8.1$ Hz, 2H), 7.38–7.30 (m, 4H), 7.27 (t, $J = 6.8$ Hz, 1H), 3.83–3.70 (m, 1H), 3.49 (s, 2H), 2.84 (d, $J = 11.5$ Hz, 2H), 2.03 (t, $J = 14.4$ Hz, 2H), 1.79 (d, $J = 11.1$ Hz, 2H), 1.59 (qd, $J = 12.1$, 3.2 Hz, 2H). ^{13}C NMR (125 MHz, DMSO) δ 165.03, 139.13, 136.28, 133.97, 129.69, 129.19, 128.69, 128.62, 127.31, 62.60, 52.69, 47.54, 31.93. ESI-MS *m/z*: 329.13 $[M + H]^+$; HRMS: calcd for $C_{19}H_{21}ClN_2O$ $[M + H]^+$ 329.1415, found 329.1416.

*N-(1-benzylpiperidin-4-yl)-5-chloropicolinamide (**w3**).* Yield 65%, yellow solid, m.p. 74–76 °C; IR (KBr) ν 3315, 2945, 2789, 1656, 1527, 1469, 1079, 771, 707, 652 cm^{-1}; ^1H NMR (500 MHz, DMSO) δ 8.70 (d, $J = 2.2$ Hz, 1H), 8.59 (d, $J = 8.4$ Hz, 1H), 8.13 (dd, $J = 8.4$, 2.4 Hz, 1H), 8.05 (d, $J = 8.4$ Hz, 1H), 7.39–7.29 (m, 4H), 7.26 (t, $J = 6.8$ Hz, 1H), 3.89–3.70 (m, 1H), 3.48 (s, 2H), 2.81 (d, $J = 11.6$ Hz, 2H), 2.07 (t, $J = 11.0$ Hz, 2H), 1.77 (d, $J = 10.9$ Hz, 2H), 1.66 (qd, $J = 12.1$, 3.5 Hz, 2H). 13C NMR (125 MHz, DMSO) δ 162.95, 148.94, 147.47, 138.04, 134.36, 129.96, 129.64, 128.72, 127.67, 123.89, 62.26, 52.36, 46.91, 31.22. ESI-MS *m/z*: 330.11 $[M + H]^+$; HRMS: calcd for $C_{18}H_{21}ClN_3O$ $[M + H]^+$ 330.1368, found 330.1365.

*N-(1-benzylpiperidin-4-yl)nicotinamide (**w4**).* Yield 75%, yellow solid, m.p. 133–135 °C; IR (KBr) ν 3294, 2917, 2793, 1632, 1551, 1063, 742, 701, 660 cm^{-1}; ^1H NMR (500 MHz, DMSO) δ 9.01 (s, 1H), 8.71 (d, $J = 3.6$ Hz, 1H), 8.46 (d, $J = 7.5$ Hz, 1H), 8.19 (d, $J = 7.9$ Hz, 1H), 7.50 (dd, $J = 7.9$, 4.8 Hz, 1H), 7.37–7.30 (m, 5H), 7.27 (t, $J = 6.4$ Hz, 1H), 3.81 (qd, $J = 11.7$, 5.7 Hz, 1H), 3.49 (s, 2H), 2.84 (d, J = 11.7 Hz, 2H), 2.05 (t, J = 10.9 Hz, 2H), 1.82 (d, J = 10.9 Hz, 2H), 1.60 (qd, $J = 12.1$, 3.5 Hz, 2H). ^{13}C NMR (125 MHz, DMSO) δ 164.78, 152.16, 148.84, 139.01, 135.52, 130.67, 129.26, 128.64, 127.36, 123.86, 62.58, 52.60, 47.53, 31.84. ESI-MS *m/z*: 296.10 $[M + H]^+$; HRMS: calcd for $C_{18}H_{22}N_3O$ $[M + H]^+$ 296.1757, found 296.1755.

*N-(1-benzylpiperidin-4-yl)-5-chlorothiophene-2-carboxamide (**w5**).* Yield 78%, pale white, solid m.p. 174–176 °C; IR (KBr) ν 3299, 2924, 1613, 1554, 1454, 742, 701 cm^{-1}; ^1H NMR (500 MHz, DMSO) δ 8.34 (d, $J = 7.6$ Hz, 1H), 7.68 (d, $J = 4.0$ Hz, 1H), 7.37–7.30 (m, 4H), 7.26 (t, $J = 6.8$ Hz, 1H), 7.18 (d, $J = 4.0$ Hz, 1H), 3.78–3.66 (m, 1H), 3.48 (s, 2H), 2.83 (d, $J = 11.4$ Hz, 2H), 2.03 (t, $J = 11.4$ Hz, 2H), 1.79 (d, $J = 10.9$ Hz, 2H), 1.57 (qd, $J = 12.1$, 3.4 Hz, 2H). ^{13}C NMR (125 MHz, DMSO) δ 160.12, 139.54, 138.65, 133.43, 129.38, 128.64, 128.43, 128.36, 127.42, 62.50, 52.49, 47.57, 31.70. ESI-MS *m/z*: 335.07 $[M + H]^+$; HRMS: calcd for $C_{17}H_{20}ClN_2OS$ $[M + H]^+$ 335.09, found 335.0977.

*N-(2-(1-benzylpiperidin-4-yl)ethyl)benzamide (**w6**).* Yield 58%, yellow solid, m.p. 94–96 °C; IR (KBr) ν 3314, 2924, 1631, 1535, 1490, 1435, 802, 774, 695 cm^{-1}; ^1H NMR (500 MHz, DMSO) δ 8.42 (t, $J = 5.3$ Hz, 1H), 7.85 (d, $J = 7.3$ Hz, 2H), 7.52 (t, $J = 7.3$ Hz, 1H), 7.47 (t, $J = 7.3$ Hz, 2H), 7.36–7.27 (m, 4H), 7.25 (t, $J = 6.9$ Hz, 1H), 3.44 (s, 2H), 3.30 (dd, J = 13.3, 6.9 Hz, 2H), 2.79 (d, J = 11.3 Hz, 2H), 1.90 (t, $J = 11.0$ Hz, 2H), 1.68 (d, $J = 12.0$ Hz, 2H), 1.48 (d, $J = 7.2$ Hz, 2H), 1.33–1.28 (m, 1H), 1.17 (qd, $J = 12.3$, 3.4 Hz, 2H). ^{13}C NMR (125 MHz, DMSO) δ 166.56, 139.17, 135.26, 131.40, 129.21, 128.67, 128.55, 127.58, 127.22, 63.02, 53.75, 37.40, 36.39, 33.52, 32.38. ESI-MS *m/z*: 323.19 $[M + H]^+$; HRMS: calcd for $C_{21}H_{27}N_2O$ $[M + H]^+$ 323.2118, found 323.2116.

*N-(2-(1-benzylpiperidin-4-yl)ethyl)-2-chlorobenzamide (**w7**).* Yield 70%, white solid, m.p. 145–147 °C; IR (KBr) ν 3276, 2918, 1640, 1553, 1452, 763, 733, 709 cm^{-1}; ^1H NMR (500 MHz, DMSO) δ 8.37 (t, $J = 5.2$ Hz, 1H), 7.50 (d, $J = 7.9$ Hz, 1H), 7.46–7.42 (m, 1H), 7.39 (d, $J = 4.2$ Hz, 2H), 7.35–7.29 (m, 4H), 7.25 (t, $J = 6.9$ Hz, 1H), 3.45 (s, 2H), 3.27 (dd, $J = 13.0$, 6.9 Hz, 2H), 2.80 (d, $J = 11.3$ Hz, 2H), 1.90 (t, $J = 10.9$ Hz, 2H), 1.67 (d, $J = 12.0$ Hz, 2H), 1.46 (q, $J = 6.9$ Hz, 2H), 1.42–1.34 (m, 1H), 1.17 (qd, $J = 12.3$, 3.4 Hz, 2H). ^{13}C NMR (125 MHz, DMSO) δ 166.65, 139.10, 137.78, 131.02, 130.27, 130.00, 129.26, 129.19, 128.56, 127.54, 127.25, 63.01, 53.78, 37.06, 36.04, 33.26, 32.27. ESI-MS *m/z*: 357.16 $[M + H]^+$; HRMS: calcd for $C_{21}H_{26}ClN_2O$ $[M + H]^+$ 357.1728, found 357.1727.

*N-(2-(1-benzylpiperidin-4-yl)ethyl)-2-(2-bromophenyl)acetamide (**w8**).* Yield 58%, yellow solid, m.p(0).83–85 °C; IR (KBr) ν 3124, 2921, 1646, 1546, 1448, 1057, 755, 660 cm^{-1}; ^1H NMR (500 MHz, DMSO) δ 7.98 (t, $J = 5.1$ Hz, 1H), 7.59 (d, $J = 8.1$ Hz, 1H), 7.37–7.28 (m, 6H), 7.26 (t, $J = 6.9$ Hz, 1H), 7.22–7.17 (m, 1H), 3.58 (s, 2H), 3.46 (s, 2H), 3.12 (dd, $J = 12.7$, 6.8 Hz, 2H), 2.80 (d, $J = 11.0$ Hz, 2H), 1.91 (t, $J = 11.0$ Hz, 2H), 1.63 (d, $J = 12.2$ Hz, 2H), 1.37 (dd, $J = 13.6$, 6.8 Hz, 2H), 1.32–1.29 (m, 1H), 1.14 (qd, $J = 12.4$ Hz, 3.5 Hz, 2H). ^{13}C NMR (125 MHz, DMSO) δ 169.30, 138.53, 135.69, 132.71, 132.32, 129.44, 129.08, 128.57, 128.02, 127.37, 122.17, 62.87, 53.59, 42.88, 36.79, 36.05, 33.05, 31.99. ESI-MS *m/z*: 415.08 $[M + H]^+$; HRMS: calcd for $C_{22}H_{27}BrN_2O$ $[M + H]^+$ 415.1380, found 415.1378.

*2-benzoyl-N-(2-(1-benzylpiperidin-4-yl)ethyl)benzamide (**w9**).* Yield 65%, white solid, m.p. 144–146 °C; IR (KBr) ν 3294, 2963, 1678, 1261, 800, 698 cm^{-1}; 1H NMR (500 MHz, DMSO) δ 7.72 (d, $J = 7.0$ Hz, 1H), 7.59–7.49 (m, 2H), 7.39–7.29 (m, 7H), 7.29–7.21 (m, 4H), 3.41 (s, 2H), 3.40–3.35 (m, 2H), 2.71 (d, $J = 2.4$ Hz, 2H), 1.84 (dd, $J = 19.7$, 9.2 Hz, 2H), 1.60 (d, $J = 12.4$ Hz, 1H), 1.48 (d, $J = 12.4$ Hz, 1H), 1.44–1.32 (m, 1H), 1.32–1.21 (m, 1H), 1.15 (dd, $J = 6.9$, 3.6 Hz, 1H), 1.00 (qd, $J = 11.7$, 3.1 Hz, 2H). ^{13}C NMR (125 MHz, DMSO) δ 167.11, 150.09, 140.72, 138.85, 132.84, 131.15, 129.61, 129.29, 128.87, 128.56, 128.51, 127.29, 126.32, 123.16, 122.80, 62.88, 53.52, 37.08, 35.26, 33.44, 32.16. ESI-MS *m/z*: 427.20 $[M + H]^+$; HRMS: calcd for $C_{28}H_{31}N_2O_2$ $[M + H]^+$ 427.2380, found 427.2379.

*N-(2-(1-benzylpiperidin-4-yl)ethyl)-3-nitrobenzamide (**w10**).* Yield 75%, yellow solid, m.p. 125–127 °C; IR (KBr) ν 3353, 2923, 1638, 1530, 1350, 821, 724 cm^{-1}; ^1H NMR (500 MHz, DMSO) δ 8.81 (t, $J = 5.3$ Hz, 1H), 8.68 (s, 1H), 8.39 (dd, $J = 8.0$, 1.7 Hz, 1H), 8.30 (d, $J = 8.0$ Hz, 1H), 7.79 (t, $J = 8.0$ Hz, 1H), 7.36–7.27 (m, 4H), 7.25 (t, $J = 7.0$ Hz, 1H), 3.45 (s, 2H), 3.35 (dd, $J = 11.8$, 4.5 Hz, 2H), 2.80 (d, $J = 11.0$ Hz, 2H), 1.91 (t, $J = 11.0$ Hz, 2H), 1.67 (t, $J = 15.3$ Hz, 2H), 1.51 (dd, $J = 14.2$, 7.0 Hz, 2H), 1.36–1.32 (m, 1H), 1.19 (qd, $J = 12.2$, 3.5 Hz, 2H). ^{13}C NMR (125 MHz, DMSO) δ 164.40, 148.28,

139.53, 136.53, 134.05, 130.54 (s), 129.22, 128.55, 127.24, 126.14, 122.32, 62.97, 53.70, 37.65, 36.17, 33.44, 32.31. ESI-MS *m/z*: 368.19 $[M+H]^+$; HRMS: calcd for $C_{21}H_{26}N_3O_3$ $[M+H]^+$ 368.1969, found 368.1970.

N-(2-(1-benzylpiperidin-4-yl)ethyl)-4-nitrobenzamide ***(w11)***. Yield 73%, yellow solid, m.p. 113–115 °C; IR (KBr) ν 3330, 2928, 1644, 1597, 1542, 1518, 741, 726, 698 cm^{-1}; ^1H NMR (500 MHz, DMSO) δ 8.76 (t, $J=5.2$ Hz, 1H), 8.32 (d, $J=8.7$ Hz, 2H), 8.07 (d, $J=8.7$ Hz, 2H), 7.35–7.27 (m, 4H), 7.25 (t, $J=6.9$ Hz, 1H), 3.45 (s, 2H), 3.34 (d, $J=11.5$ Hz, 2H), 2.80 (d, $J=11.0$ Hz, 2H), 1.91 (t, $J=11.0$ Hz, 2H), 1.68 (d, $J=12.0$ Hz, 2H), 1.50 (dd, $J=14.1$, 7.0 Hz, 2H), 1.34–1.31 (m, 1H), 1.18 (qd, $J=12.2$, 3.5 Hz, 2H). ^{13}C NMR (126 MHz, DMSO) δ 164.99, 149.40, 140.81, 139.06, 129.24, 129.09, 128.55, 127.24, 123.95, 62.98, 53.69, 37.65, 36.13, 33.46, 32.28. ESI-MS *m/z*: 368.18 $[M+H]^+$; HRMS: calcd for $C_{21}H_{26}N_3O_3$ $[M+H]^+$ 368.1969, found 368.1968.

N-(2-(1-benzylpiperidin-4-yl)ethyl)-4-methoxybenzamide ***(w12)***. Yield 75%, yellow solid, m.p. 125–127 °C; IR (KBr) ν 3293, 2918, 1627, 1558, 1509, 1255, 843, 736, 673 cm^{-1}; ^1H NMR (500 MHz, DMSO) δ 8.26 (t, $J=5.3$ Hz, 1H), 7.82 (d, $J=8.8$ Hz, 2H), 7.35–7.28 (m, 5H), 7.25 (t, $J=6.9$ Hz, 1H), 6.99 (d, $J=8.8$ Hz, 2H), 3.82 (s, 3H), 3.44 (s, 2H), 3.28 (dd, $J=13.4$, 6.6 Hz, 2H), 2.79 (d, $J=11.3$ Hz, 2H), 1.90 (t, $J=10.9$ Hz, 2H), 1.68 (d, $J=11.7$ Hz, 2H), 1.47 (dd, $J=14.1$, 6.9 Hz, 2H), 1.32–1.28 (m, 1H), 1.17 (qd, $J=12.3$, 3.4 Hz, 2H). ^{13}C NMR (125 MHz, DMSO) δ 166.13, 161.90, 139.04, 129.38, 129.27, 128.56, 127.43, 127.26, 113.91, 62.98, 55.80, 53.72, 37.33, 36.43, 33.49, 32.31. ESI-MS *m/z*: 353.20 $[M+H]^+$; HRMS: calcd for $C_{22}H_{29}N_2O$ $[M+H]^+$ 353.2224, found 353.2222.

N-(2-(1-benzylpiperidin-4-yl)ethyl)-4-methylbenzamide ***(w13)***. Yield 77%, yellow solid m.p. 85–92 °C; IR (KBr) ν 3321, 2925, 1633, 1550, 1453, 1311, 730, 697 cm^{-1}; ^1H NMR (500 MHz, DMSO) δ 8.31 (t, $J=5.4$ Hz, 1H), 7.75 (d, $J=8.1$ Hz, 2H), 7.35–7.29 (m, 4H), 7.25–7.23 (m, 3H), 3.45 (s, 2H), 3.29 (dd, $J=13.4$, 6.9 Hz, 2H), 2.79 (d, $J=11.0$ Hz, 2H), 2.36 (s, 3H), 1.92 (t, $J=11.0$ Hz, 2H), 1.68 (d, $J=11.9$ Hz, 2H), 1.47 (dd, $J=14.2$, 6.9 Hz, 2H), 1.33–1.29 (m, 1H), 1.17 (qd, $J=12.2$, 3.4 Hz, 2H). ^{13}C NMR (125 MHz, DMSO) δ 166.40, 141.21, 139.07, 132.44, 129.23, 129.18, 128.55, 127.59, 127.25, 62.95, 53.72, 37.32, 36.40, 33.49, 32.33, 21.38. ESI-MS *m/z*: 337.21 $[M+H]^+$; HRMS: calcd for $C_{22}H_{29}N_2O$ $[M+H]^+$ 337.2274, found 337.2273.

N-(2-(1-benzylpiperidin-4-yl)ethyl)-4-chlorobenzamide ***(w14)***. Yield 88%, yellow solid, m.p. 122–124 °C; IR (KBr) ν 3305, 2914, 1632, 1543, 845, 743, 701 cm^{-1}; ^1H NMR (500 MHz, DMSO) δ 8.49 (t, $J=5.3$ Hz, 1H), 7.86 (d, $J=8.5$ Hz, 2H), 7.54 (d, $J=8.5$ Hz, 2H), 7.37–7.27 (m, 4H), 7.25 (t, $J=6.7$ Hz, 1H), 3.44 (s, 2H), 3.30 (dd, $J=13.4$, 6.7 Hz, 2H), 2.79 (d, $J=11.0$ Hz, 2H), 1.91 (t, $J=11.0$ Hz, 2H), 1.68 (d, $J=11.9$ Hz, 2H), 1.48 (dd, $J=14.1$, 7.0 Hz, 2H), 1.32–1.29 (m, 1H), 1.17 (qd, $J=12.2$, 3.4 Hz, 2H). ^{13}C NMR (125 MHz, DMSO) δ 165.59, 136.32, 135.07, 133.89, 129.53, 129.41, 128.80, 128.61, 127.43, 62.77, 53.59, 37.44, 36.19, 33.31, 32.08. ESI-MS *m/z*: 357.16 $[M+H]^+$; HRMS: calcd for $C_{21}H_{26}ClN_2O$ $[M+H]^+$ 357.1728, found 357.1727.

N-(2-(1-benzylpiperidin-4-yl)ethyl)quinoline-2-carboxamide ***(w15)***. Yield 85%, yellow solid, m.p. 95–97 °C; IR (KBr) ν 3382, 2938, 1667, 1522, 1496, 781, 737, 697 cm^{-1}; ^1H NMR (500 MHz, DMSO) δ 8.90 (t, $J=5.9$ Hz, 1H), 8.57 (d, $J=8.5$ Hz, 1H), 8.18–8.14 (m, 2H), 8.10 (d, $J=8.0$ Hz, 1H), 7.89 (dd, $J=11.2$, 4.1 Hz, 1H), 7.74 (t, $J=7.5$ Hz, 1H), 7.35–7.27 (m, 4H), 7.25 (t, $J=6.8$ Hz, 1H), 3.42 (dd, $J=15.6$, 8.2 Hz, 4H), 2.80 (d, $J=11.0$ Hz, 2H), 1.91 (t, $J=11.0$ Hz, 2H), 1.72 (d, $J=12.1$ Hz, 2H), 1.55 (dd, $J=14.2$, 7.0 Hz, 2H), 1.37–1.29 (m, 1H), 1.17 (qd, $J=12.1$, 3.3 Hz, 2H). ^{13}C NMR (125 MHz, DMSO) δ 164.40, 150.78, 146.48, 138.28, 130.94, 129.94, 129.65, 129.33, 129.23, 128.58, 128.53, 128.46, 127.35, 119.09, 62.85, 53.62, 37.20, 36.45, 33.42, 32.18. ESI-MS *m/z*: 374.21 $[M+H]^+$; HRMS: calcd for $C_{24}H_{28}N_3O$ $[M+H]^+$ 374.2227, found 374.2226.

N-(2-(1-benzylpiperidin-4-yl)ethyl)nicotinamide ***(w16)***. Yield 65%, yellow solid, m.p. 64–66 °C; IR (KBr) ν 3306, 2925, 1636, 1548, 1311, 731, 707, 663 cm^{-1}; ^1H NMR (500 MHz, DMSO) δ 9.00 (s, 1H), 8.71 (dd, $J=4.8$, 1.4 Hz, 1H), 8.61 (t, $J=5.2$ Hz, 1H), 8.18 (dt, $J=7.9$, 1.8 Hz, 1H), 7.51 (dd, $J=7.9$, 4.8 Hz, 1H), 7.35–7.28 (m, 5H), 7.25 (t, $J=6.9$ Hz, 1H), 3.44 (s, 2H), 3.31 (d, $J=6.9$ Hz, 2H), 2.79 (d, $J=11.9$ Hz, 2H), 1.91 (t, $J=10.8$ Hz, 2H), 1.68 (d, $J=11.9$ Hz, 2H), 1.49 (dd, $J=14.2$, 7.0 Hz, 2H), 1.35–1.30 (m, 1H), 1.18 (qd, $J=12.2$, 3.5 Hz, 2H). ^{13}C NMR (125 MHz, DMSO) δ 165.14, 152.13, 148.73, 135.34, 129.28, 128.56, 127.29, 123.89, 62.92, 53.67, 37.42, 36.20, 33.42, 32.24. ESI-MS *m/z*: 324.18 $[M+H]^+$; HRMS: calcd for $C_{20}H_{26}N_3O$ $[M+H]^+$ 324.2070, found 324.2068.

N-(2-(1-benzylpiperidin-4-yl)ethyl)isonicotinamide ***(w17)***. Yield 78%, yellow oil; IR (KBr) ν 3294, 2925, 1648, 1551, 1451, 1309, 1065, 742, 701, 660 cm^{-1}; ^1H NMR (500 MHz, DMSO) δ 8.73 (d, $J=5.8$ Hz, 1H), 7.75 (d, $J=5.8$ Hz, 1H), 7.35–7.27 (m, 4H), 7.25 (t, $J=6.9$ Hz, 1H), 7.03 (s, 1H), 3.44 (s, 2H), 3.33–3.29 (m, 2H), 2.79 (d, $J=11.3$ Hz, 2H), 1.96–1.86 (m, 2H), 1.66 (t, $J=14.0$ Hz, 1H), 1.49 (dd, $J=14.0$, 6.9 Hz, 1H), 1.34–1.28 (m, 1H), 1.18 (qd, $J=12.1$, 3.5 Hz, 2H). ^{13}C NMR (125 MHz, DMSO) δ 165.04, 150.63, 142.07, 138.88, 129.29, 128.57, 127.30, 121.65, 62.91, 53.64, 37.50, 36.09, 33.40, 32.20. ESI-MS *m/z*: 324.18 $[M+H]^+$; HRMS: calcd for $C_{20}H_{26}N_3O$ $[M+H]^+$ 324.2070, found 324.2071.

N-(2-(1-benzylpiperidin-4-yl)ethyl)-5-chloropicolinamide ***(w18)***. Yield 66%, yellow solid, m.p. 65–69 °C; IR (KBr) ν 3415, 3301, 2930, 2855, 1663, 1533, 1455, 1110, 790, 732, 684 cm^{-1}; ^1H NMR (500 MHz, DMSO) δ 8.80 (t, $J=5.8$ Hz, 1H), 8.70 (d, $J=2.2$ Hz, 1H), 8.13 (dd, $J=8.4$, 2.4 Hz, 1H), 8.04 (d, $J=8.4$ Hz, 1H), 7.38–7.28 (m, 4H), 7.26 (t, $J=6.9$ Hz, 1H), 3.47 (s, 2H), 3.34–3.30 (m, 2H), 2.80 (d, $J=8.7$ Hz, 2H), 1.92 (s, 2H), 1.69 (d, $J=12.3$ Hz, 2H), 1.49 (dd, $J=14.0$, 6.9 Hz, 2H), 1.33–1.28 (m, 1H), 1.17 (qd, $J=12.3$, 3.4 Hz, 2H). ^{13}C NMR (125 MHz, DMSO) δ 163.38, 149.15, 147.47, 138.84, 138.84, 137.98, 134.24, 129.30, 128.56, 127.30, 123.80, 62.89, 53.64, 37.10, 36.29, 33.36, 32.18. ESI-MS *m/z*: 358.15 $[M+H]^+$; HRMS: calcd for $C_{20}H_{25}ClN_3O$ $[M+H]^+$ 358.1681, found 358.1680.

N-(2-(1-benzylpiperidin-4-yl)ethyl)-5-fluoropicolinamide ***(w19)***. Yield 55%, yellow solid, m.p. 81–83 °C; IR (KBr) ν 3306, 2928, 1661, 1530, 1469, 1227, 732, 682 cm^{-1}; ^1H NMR (500 MHz, DMSO) δ 8.71 (t, $J=5.7$ Hz, 1H), 8.64 (d, $J=2.7$ Hz, 1H), 8.11 (dd, $J=8.7$, 4.7 Hz, 1H), 7.90 (d, $J=8.7$ Hz, 1H), 7.34–7.28 (m, 4H), 7.24 (t, $J=6.9$ Hz, 1H), 3.44 (s, 2H), 3.38–3.33 (m, 2H), 2.78 (d, $J=11.2$ Hz, 2H), 1.89 (t, $J=11.2$ Hz, 2H), 1.68 (d, $J=11.2$ Hz, 2H), 1.49 (dd, $J=14.0$, 6.9 Hz, 2H), 1.31–1.26 (m, 1H), 1.16 (qd, $J=12.2$, 3.4 Hz, 2H). ^{13}C NMR (125 MHz, DMSO) δ 163.27, 160.04, 147.37, 139.03, 137.15, 129.24, 128.54, 127.24, 124.85, 124.43, 62.96, 53.68, 37.08, 36.36, 33.42, 32.26. ESI-MS *m/z*: 342.18 $[M+H]^+$; HRMS: calcd for $C_{20}H_{25}FN_3O$ $[M+H]^+$ 342.1976, found 342.1974.

*N-(2-(1-benzylpiperidin-4-yl)ethyl)-6-methylpicolinamide (**w20**).* Yield 65%, yellow oil; IR (KBr) ν 3389, 2923, 1673, 1593, 1526, 1452, 740, 699 cm^{-1}; ^1H NMR (500 MHz, DMSO) δ 8.58 (t, $J = 5.8$ Hz, 1H), 7.90–7.80 (m, 2H), 7.45 (d, $J = 7.3$ Hz, 1H), 7.36–7.27 (m, 4H), 7.25 (t, $J = 6.9$ Hz, 1H), 3.43 (s, 2H), 3.35 (d, $J = 13.7$ Hz, 2H), 2.78 (t, $J = 11.3$ Hz, 2H), 2.57 (s, 3H), 1.90 (t, $J = 11.3$ Hz, 2H), 1.69 (d, $J = 11.9$ Hz, 2H), 1.49 (dd, $J = 14.2$, 6.9 Hz, 2H), 1.31–1.23 (m, 1H), 1.17 (qd, $J = 12.1$, 3.3 Hz, 2H). ^{13}C NMR (125 MHz, DMSO) δ 164.36, 157.57, 149.84, 138.32, 129.34, 128.58, 127.31, 126.37, 119.36, 62.93, 53.64, 36.97, 36.45, 33.42, 32.16, 24.32. ESI-MS *m/z*: 338.22 $[M + H]^+$; HRMS: calcd for $C_{21}H_{28}N_3O$ $[M + H]^+$ 338.2227, found 338.2226.

*N-(2-(1-benzylpiperidin-4-yl)ethyl)-5-chlorothiophene-2-carboxamide (**w21**).* Yield 80%, yellow solid, m.p. 115–117 °C; IR (KBr) ν 3299, 2929, 1661, 1531, 1453, 1108, 730, 682 cm^{-1}; ^1H NMR (500 MHz, DMSO) δ 8.53 (t, $J = 5.4$ Hz, 1H), 7.63 (d, $J = 4.0$ Hz, 1H), 7.35–7.28 (m, 4H), 7.25 (dd, $J = 9.3$, 4.4 Hz, 1H), 7.18 (d, $J = 4.0$ Hz, 1H), 3.47 (s, 2H), 3.26 (dd, $J = 13.4$, 6.7 Hz, 2H), 2.80 (d, $J = 11.1$ Hz, 2H), 1.93 (t, $J = 11.1$ Hz, 2H), 1.67 (d, $J = 12.1$ Hz, 2H), 1.46 (dd, $J = 14.2$, 7.0 Hz, 2H), 1.31–1.29 (m, 1H), 1.17 (qd, $J = 12.3$, 3.5 Hz, 2H). ^{13}C NMR (125 MHz, DMSO) δ 160.40, 139.90, 133.07, 129.27, 128.57, 128.43, 128.08, 127.31, 62.87, 53.64, 37.30, 36.28, 33.36, 32.21. ESI-MS *m/z*: 362.12 $[M + H]^+$; HRMS: calcd for $C_{19}H_{24}ClN_2OS$ $[M + H]^+$ 363.1292, found 363.1293.

*N-(2-(1-benzylpiperidin-4-yl)ethyl)-5-bromothiophene-2-carboxamide (**w22**).* Yield 59%, yellow solid, m.p. 124–126 °C; IR (KBr) ν 3279, 2924, 1617, 1564, 1421, 1304, 736, 694 cm^{-1}; ^1H NMR (500 MHz, DMSO) δ 8.50 (t, $J = 5.4$ Hz, 1H), 7.58 (d, $J = 4.0$ Hz, 1H), 7.35–7.28 (m, 4H), 7.28 (d, $J = 4.0$ Hz, 1H), 7.25 (t, $J = 6.9$ Hz, 1H), 3.44 (s, 2H), 3.25 (dd, $J = 13.5$, 6.6 Hz, 2H), 2.79 (d, $J = 10.9$ Hz, 2H), 1.90 (t, $J = 10.9$ Hz, 2H), 1.66 (d, $J = 11.7$ Hz, 2H), 1.46 (dd, $J = 14.2$, 6.9 Hz, 2H), 1.36–1.29 (m, 1H), 1.17 (qd, $J = 12.3$, 3.3 Hz, 2H). ^{13}C NMR (125 MHz, DMSO) δ 160.40, 142.53, 139.03, 131.86, 129.24, 128.91, 128.55, 127.25, 116.81, 62.96, 53.67, 37.30, 36.27, 33.41, 32.26. ESI-MS *m/z*: 407.07 $[M + H]^+$; HRMS: calcd for $C_{19}H_{24}BrN_2OS$ $[M + H]^+$ 407.0787, found 407.0786.

*N-(2-(1-benzylpiperidin-4-yl)ethyl)-5-methylthiophene-2-carboxamide (**w23**).* Yield 66%, yellow solid, m.p. 107–110 °C; IR (KBr) ν 3281, 2923, 1616, 1562, 1449, 1308, 736, 694 cm^{-1}; ^1H NMR (500 MHz, DMSO) δ 8.27 (t, $J = 5.4$ Hz, 1H), 7.53 (d, $J = 3.5$ Hz, 1H), 7.37–7.28 (m, 4H), 7.25 (t, $J = 6.9$ Hz, 1H), 6.83 (d, $J = 3.5$ Hz, 1H), 3.45 (s, 2H), 3.24 (dd, $J = 13.4$, 6.6 Hz, 2H), 2.79 (d, $J = 11.0$ Hz, 2H), 2.46 (s, 3H), 1.91 (t, $J = 11.0$ Hz, 2H), 1.67 (d, $J = 11.9$ Hz, 2H), 1.45 (dd, $J = 14.2$, 6.9 Hz, 2H), 1.33–1.28 (m, 1H), 1.17 (qd, $J = 12.2$, 3.4 Hz, 2H). ^{13}C NMR (125 MHz, DMSO) δ 161.42, 144.60, 139.07, 138.21, 129.22, 128.55, 128.36, 127.24, 126.68, 62.96, 53.70, 37.19, 36.46, 33.44, 32.32, 15.56. ESI-MS *m/z*: 343.17 $[M + H]^+$; HRMS: calcd for $C_{20}H_{27}N_2OS$ $[M + H]^+$ 343.1839, found 343.1838.

Biological activity

Inhibitory activity against AChE and BuChE

Acetylcholinesterase (eeAChE, E.C. 3.1.1.7, from electric eel and hAChE, EC 3.1.1.7, from human erythrocyes), butyrylcholinesterase (BuChE, E.C. 3.1.1.8, from equine serum), 5,5′-dithiobis-(2-nitrobenzoic acid) (Ellman's reagent, DTNB), *S*-butyrylthiocholine iodide (BTCI), acetylthiocholine iodide (ATCI), and donepezil hydrochloride were purchased from Sigma-Aldrich (St. Louis, MO). The capacity of the test compounds (**w1**–**23**) to inhibit AChE and BuChE activities were assessed by Ellman's method. Stock solution of test compounds was dissolved in a minimum volume of DMSO (1%) and was diluted using the buffer solution (50 mM Tris-HCl, pH= 8.0, 0.1 M NaCl, 0.02 M $MgCl_2 \cdot 6H_2O$). In 96-well plates, 160 µL of 1.5 mM DTNB, 50 µL of AChE (0.22 U/mL prepared in 50 mM Tris-HCl, pH =8.0, 0.1% w/v bovine serum albumin, BSA) or 50 µL of BuChE (0.12 U/mL prepared in 50 mM Tris-HCl, pH = 8.0, 0.1% w/v BSA) were incubated with 10 µL of various concentrations of test compounds (0.001–100 µM) at 37 °C for 6 min followed by the addition of the substrates (30 µL) acetylthiocholine iodide (15 mM) or *S*-butyrylthiocholine iodide (15 mM) and the absorbance was measured at different time intervals (0, 60, 120, and 180 s) at a wavelength of 405 nm. The concentration of compound producing 50% of enzyme activity inhibition (IC_{50}) was calculated by nonlinear regression analysis of the response-concentration (log) curve, using the Graph-Pad Prism program package (Graph Pad Software, San Diego, CA). Results are expressed as the mean ± SD of at least three different experiments performed in triplicate.

Inhibitory activity against hMAO-A and hMAO-B

Monoamine Oxidases (hMAO-A, hMAO-B, E.C. 1.4.3.4), *p*-tyramine, Amplex Red and horseradish peroxidase (E.C. 1.11.1.7) were purchased from Sigma-Aldrich. Firstly, MAOs activity were adjusted to obtain in our experimental conditions the same reaction velocity in the presence of both isoforms (i.e., to oxidize (in the control group) the same concentration of substrate: 165 pmol of *p*-tyramine/min(hMAO-A: 1.1 µg protein; specific activity: 150 nmol of *p*-tyramine oxidized to *p*-hydroxyphenylacetaldehyde/min/mg protein; hMAO-B: 7.5 µg protein; specific activity: 22 nmol of *p*-tyramine transformed/min/mg protein). Then compounds were dissolved in DMSO (10 mM) and diluted in 0.05 M KH_2PO_4/K_2HPO_4 buffer (pH = 7.4) to the desired final concentration. All the compounds are soluble at the tested concentration. Test drugs (20 µL) and MAO (80 µL) were incubated at 37 °C for 15 min in a flat-black-bottom 96-well microtest plate in dark. The reaction was started by adding 200 µM Amplex Red reagent, 2 U/mL horseradish peroxidase, and 2 mM *p*-tyramine for hMAO at 37 °C for 20 min. The production of H_2O_2 and consequently, of resorufin, was quantified at 37 °C in a SpectraMax Paradigm (Molecular Devices, Sunnyvale, CA) multi-mode detection platform reader based on the fluorescence generated (excitation, 545 nm; emission, 590 nm). The specific fluorescence emission was calculated after subtraction of the background activity. The background activity was determined from wells containing all components except the MAO isoforms, which were replaced by a sodium phosphate buffer solution (0.05 mM, pH 7.4). The percent inhibition was calculated by the following expression: $(1 - IF_i/IF_c) \times 100$ in which IF_i and IF_c are the fluorescence intensities obtained for hMAO in the presence and absence of inhibitors after subtracting the respective background.

Kinetic study of AChE inbition

To obtain of the mechanism of action **w18**, reciprocal plots of 1/velocity versus 1/substrate were constructed at different concentrations of the substrate thiocholine iodide 0.05–0.5 mM by using Ellman's method. Three concentrations of **w18** were selected for the studies: 0.440, 0.220 and 0.110 µM for the kinetic analysis of AChE inhibition. The plots were assessed by a weighted least-squares analysis that assumed the variance of velocity (v) to be a constant percentage of v for the entire data set. Slopes of these reciprocal plots were then plotted against the

concentration of **w18** in a weighted analysis and K_i was determined as the intercept on the negative *x*-axis. Data analysis was performed with GraphPad Prism 4.03 software (GraphPad Software Inc., San Diego, CA).

Reversibility and kinetic studies of hMAO-B inhibition

To determine whether the inhibition of hMAO-B by the donepezil-like compounds were reversible or irreversible, the time-dependence of inhibition of the selected inhibitor **w18** and reference compound pargyline were examined. Compounds were allowed to pre-incubate with recombinant human hMAO-B for various periods of time (0, 15, 30, 60 min) at 37 °C in potassium phosphate buffer (0.05 mM, pH 7.4). The concentrations of the compounds were about twofold the measured IC_{50} values for the inhibition of hMAO-B. The reactions were subsequently diluted two-fold to yield a final enzyme concentration of 0.015 mg mL^{-1} and concentrations of the inhibitors that are about equal to the IC_{50} values. The reactions were incubated at 37 °C for a further 15 min. All measurements were carried out in triplicate and are expressed as mean ± SD.

Then, the type of hMAO-B inhibition was determined by constructing a set of Lineweaver–Burk plots. Six different concentrations of the substrate *p*-tyramine (0.05, 0.1, 0.25, 0.33, 0.5, and 1.0 mM) was applied, and the initial catalytic rates of hMAO-B were measured in the absence and in the presence of three different concentrations (6.28, 3.14, and 1.57 μM) of compound **w18**. The assay conditions and measurements were similar to the IC_{50} determination. The plots were assessed by a weighted leastsquares analysis that assumed the variance of velocity (v) to be a constant percentage of v for the entire data set. Slopes of these reciprocal plots were then plotted against the concentration of **w18** in a weighted analysis. Data analysis was performed with GraphPad Prism 4.03 software (San Diego, CA).

*Molecular modeling studies of **w18** with ChEs and hMAO-B*

Molecular modeling calculations and docking studies were performed using Molecular Operating Environment (MOE) software version 2008.10 (Chemical Computing Group, Montreal, Canada). The X-ray crystallographic structure of AChE in complexed with donepezil (PDB code 1EVE), hBuChE (PDB code 1P0I) and human MAO-B in complexed with 7-(3-chlorobenzyloxy)-4-formylcoumarin (PDB code 2V60) were obtained from the Protein Data Bank. All water molecules in PDB files were removed and hydrogen atoms were subsequently added to the protein. The compound **w18** was built using the builder interface of the MOE program and energy minimized using MMFF94x forcefield. Then the **w18** was docked into the active site of the protein by the ''Triangle Matcher'' method, which generated poses by aligning the ligand triplet of atoms with the triplet of alpha spheres in cavities of tight atomic packing. The Dock scoring in MOE software was done using ASE scoring function and forcefield was selected as the refinement method. The best 10 poses of molecules were retained and scored. After docking, the geometry of resulting complex was studied using the MOE's pose viewer utility.

Spectrophotometric measurement of complex with Cu^{2+}

The study of metal chelation was performed in methanol at 298 K using UV–Vis spectrophotometer (SHIMADZU UV-2450PC) with wavelength ranging from 200 to 500 nm. The difference UV–Vis spectra due to complex formation was obtained by numerical subtraction of the spectra of the metal ions alone and the compound alone (at the same concentration used in the mixture) from the spectra of the mixture. A fixed amount of **w18** (50 μM) was mixed with growing amounts of metal ions (10–80 μM).

In vitro *BBB permeation assay*

Brain penetration of compounds was evaluated using a parallel artificial membrane permeation assay (PAMPA). Commercial drugs were purchased from Sigma and Alfa Aesar. The porcine brain lipid (PBL) was obtained from Avanti Polar Lipids. The donor microplate (PVDF membrane, pore size 0.45 mm) and the acceptor microplate were both from Millipore (St. Charles, MO). The 96-well UV plate (COSTAR®) was from Corning Incorporated. The acceptor 96-well microplate was filled with 300 μL of PBS:EtOH (7:3), and the filter membrane was impregnated with 4 μL of PBL in dodecane (20 mg/mL). Compounds were dissolved in DMSO at 5 mg/mL and diluted 50-fold in PBS/EtOH (7:3) to achieve a concentration of 100 mg/mL, 200 μL of which was added to the donor wells. The acceptor filter plate was carefully placed on the donor plate to form a sandwich, which was left undisturbed for 16 h at 25 °C. After incubation, the donor plate was carefully removed and the concentration of compound in the acceptor wells was determined using a UV plate reader (Flexsta-tion® 3). Every sample was analyzed at five wavelengths, in four wells, in at least three independent runs, and the results are given as the mean ± standard deviation. In each experiment, 9 quality control standards of known BBB permeability were included to validate the analysis set.

Rat pheochromocytoma (PC12) cell toxicity

The toxicity effect of compounds on the rat pheochromocytoma (PC12) cells was examined. The PC12 cells were routinely grown at 37 °C in a humidified incubator with 5% CO_2 in Dulbecco's modified Eagle's medium (DMEM) supplemented with 10% bovine calf serum, 100 units/mL penicillin, and 100 units/mL of streptomycin. Cells were subcultured in 96-well plates at a seeding density of 10 000 cells per well and allowed to adhere and grow. When cells reached the required confluence, they were placed into serum-free medium and treated with compound **w18**. Twenty-four hours later the survival of cells was determined by MTT assay. Briefly, after incubation with 20 μL of MTT at 37 °C for 4 h, living cells containing MTT formazan crystals were solubilized in 200 μL DMSO. The absorbance of each well was measured using a microculture plate reader with a test wavelength of 570 nm and a reference wavelength of 630 nm. Results are expressed as the mean ± SD of three independent experiments.

Results and discussion

Chemistry

The synthetic route for target compounds is shown in Scheme 1. Activation of different carboxylic acid compounds with 1,1′-carbonyldiimidazole (CDI) and subsequent coupling to 1-benzylpiperidin-4-amine or 2-(1-benzylpiperidin-4-yl) ethanamine afforded target compounds **w1**–**23** in good yields[46–48]. Structures of all synthesized compounds were characterized by ^1H and ^{13}C nuclear magnetic resonance (NMR) spectroscopy (see Supplementary data).

Inhibitory activity against AChE and BuChE

To determine the potential interest of the new donepezil-like compounds for the treatment of AD, the ChEs inhibitory activities were assayed by the method of Ellmam et al. using donepezil and galanthamine as reference compounds[49]. The AChE inhibitory

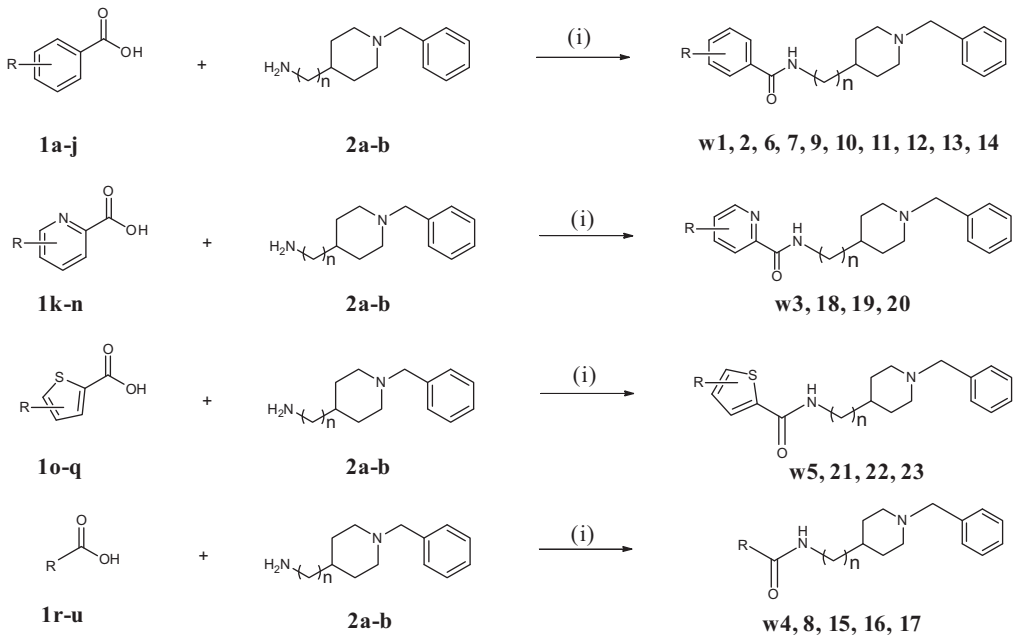

1a R = H
1b R = 2-Cl
1c R = 2-NO_2
1d R = 2-Ph CO
1e R = 3-NO_2
1f R = 3-Cl
1g R = 4-NO_2
1h R = 4-OCH_3
1i R = 4-CH_3
1J R = 4-Cl
1k R = 3-Cl
1l R = 5-Cl
1m R = 5-F
1n R = 6-CH_3
1o R = 5-Cl
1p R = 5-Br
1q R = 5-CH_3
1r R = 2-quinoline
1s R = 2-Br $PhCH_2$
1t R = 3-pyridine
1u R = 4-pyridine

2a n = 0
2b n = 2

w1 R = H, n = 0
w2 R = 3-Cl, n = 0
w3 R = 3-Cl, n = 0
w4 R = 3-pyridine, n = 0
w5 R =5-Cl, n = 0
w6 R = H, n = 2
w7 R = 2-Cl, n = 2
w8 R = 2-Br $PhCH_2$, n = 2
w9 R = 2-Ph CO, n = 2
w10 R = 3-NO_2, n = 2
w11 R = 4-NO_2, n = 2
w12 R = 4-OCH_3, n = 2
w13 R = 4-CH_3, n = 2
w14 R = 4-Cl, n = 2
w15 R = 2-quinoline, n = 2
w16 R = 3-pyridine, n = 2
w17 R = 4-pyridine, n = 2
w18 R = 5-Cl, n = 2
w19 R = 5-F, n = 2
w20 R = 6-CH_3, n = 2
w21 R = 5-Cl, n = 2
w22 R = 5-Br, n = 2
w23 R = 5-CH_3, n = 2

Scheme 1. Reagents and conditions: (i) 1,1′-carbonyldiimidazole (CDI), CH_2Cl_2, r.t. overnight.

was tested against the *Electrophorus electricus* enzyme (eeAChE), and the inhibition of BuChE was carried out using the equine serum enzyme (eqBuChE). The IC_{50} values of all tested compounds and their slectivity index for AChE over BuChE are summarized in Table 1.

From the table, it can be seen that most of our target compounds showed potent inhibitory activity to both ChEs with IC_{50} values ranging from micromolar to nanomolar. The length of linker of the new compounds has great influences on the inhibitory activities. From the IC_{50} values, compounds **w6–23** with *N*-ethylcarboxamide linkage exhibited a higher activity than those **w1–5** with carboxamide linkage. This suggested that the suitable linker length seemed to be 2 carbon atoms for ChEs inhibition. Then, the introduction of substituents with different sizes to phenyl ring and pyridine ring were planned. Among compounds **w6–20**, **w11** (IC_{50} = 0.123 μM) showed the highest inhibitory activity against AChE, which was 20 times stronger than that of reference compound galanthamine (IC_{50} = 2.67 μM), and 3 times less than that of donepzil (IC_{50} = 0.035 μM). Compound **w8** exhibited strongest inhibition against BuChE with IC_{50} value of 0.323 μM, which was 7 times more potent than that of donepezil (IC_{50} = 2.32 μM), and showed the highest selectivity with a selectivity index of 0.0392. Compared with the unsubstituted compound **w6** (IC_{50} = 1.51 μM for AChE; IC_{50} = 1.82 μM for BuChE), introduction of Cl or NO_2 group on the 4-position of phenyl ring (**w11**, **w14**), showed inhibitory activities for both ChEs better than those of compound **w6**. On the contrary, incorporating the benzoyl group in the 2-position of phenyl ring (**w9**) showed a decreased ChEs inhibitory activities (IC_{50} = 52.2 μM for AChE; IC_{50} = 3.57 μM for BuChE). This might be attributed to the steric hindrance of the benzoyl group. Moreover, different substituents were introduced to the 5- or 6-position of pyridine ring, most of them showed good inhibitory activity against AChE. Especially, the inhibitory activities of **w18** against AChE and BuChE (IC_{50} = 0.220 μM for AChE; IC_{50} = 1.23 μM for BuChE) were 12-fold and 10-fold more potent, respectively, than those of reference compound galanthamine (IC_{50} = 2.67 μM for AChE; IC_{50} = 12.7 μM for BuChE). To extend the series of our compounds, compounds **w21–23** with thiophene moiety were synthesized. As the trend with **w21–23** for AChE inhibition, **w21–23** were also sensitive to the size of substituents at 5-position of thiophene ring. For example, the AChE inhibitory activity of **w21** (IC_{50} = 0.269 μM) for was 6-fold more potent than that of **w23** (IC_{50} = 1.55 μM). However, BuChE inhibitory activities of **w21–23** seemed to be the opposite trend compared with the AChE inhibitory activities, inhibitory activity of **w22** for BuChE (IC_{50} = 0.208 μM) was 13-fold more potent than that of **w21** (IC_{50} = 2.75 μM). This suggested the thiophene ring also might be favorable for ChEs inhibition.

Table 1. Cholinesterases and human recombinant MAO isoforms inhibitory activities of tested compounds and reference compounds.

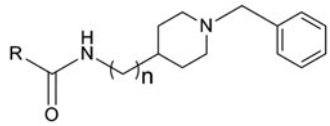

			IC_{50}[a] (μM)		Selectivity index	IC_{50}[a] (μM)		Selectivity index
Compound	R	n	eeAChE	eqBuChE	eqBuChE/eeAChE	hMAO-A	hMAO-B	hMAO-A/hMAO-B
w1	Ph	0	76.6 ± 4.5	70.4 ± 3.2	0.92	N	N	–
w2	3-Cl Ph	0	80.7 ± 4.0	N[b]	>1.24	N	N	–
w3	3-Cl-2-pyridine	0	9.95 ± 0.12	58.7 ± 2.7	5.90	N	N	–
w4	3-Pyridine	0	54.2 ± 2.9	N	>1.85	N	N	–
w5	5-Cl-2-thiophene	0	23.6 ± 1.5	N	>4.34	N	N	–
w6	Ph	2	1.51 ± 0.22	1.82 ± 0.08	1.21	N	N	–
w7	2-Cl Ph	2	1.86 ± 0.09	2.49 ± 0.14	1.34	N	N	–
w8	2-Br $PhCH_2$	2	8.23 ± 0.34	0.323 ± 0.033	0.0392	N	46.8 ± 2.2	>2.14
w9	2-(PhCO) Ph	2	52.2 ± 1.3	3.57 ± 0.14	0.0684	N	N	–
w10	3-NO_2 Ph	2	0.298 ± 0.031	0.918 ± 0.080	3.08	92.4 ± 7.1	26.2 ± 1.5	>3.53
w11	4-NO_2 Ph	2	0.123 ± 0.022	0.570 ± 0.035	4.63	22.6 ± 1.8	68.3 ± 4.0	0.331
w12	4-OCH_3 Ph	2	0.662 ± 0.029	1.26 ± 0.11	2.03	N	N	–
w13	4-CH_3 Ph	2	1.45 ± 0.07	1.65 ± 0.08	1.14	N	94.1 ± 4.9	1.06
w14	4-Cl Ph	2	0.378 ± 0.015	0.620 ± 0.07	1.64	23.2 ± 1.8	9.27 ± 1.3	2.5
w15	2-quinoline	2	0.174 ± 0.009	0.601 ± 0.06	3.54	24.5 ± 2.3	48.6 ± 3.3	0.504
w16	3-pyridine	2	0.791 ± 0.045	13.6 ± 0.6	17.2	N	N	–
w17	4-pyridine	2	0.340 ± 0.031	5.40 ± 0.27	15.9	N	N	–
w18	5-Cl-2-pyridine	2	0.220 ± 0.006	1.23 ± 0.10	5.6	13.4 ± 0.9	3.14 ± 027	4.27
w19	5-F-2-pyridine	2	0.502 ± 0.011	3.85 ± 0.27	15.3	N	N	–
w20	6-CH_3-2-pyridine	2	0.434 ± 0.019	3.64 ± 0.18	8.39	N	2.53 ± 1.4	>39.5
w21	5-Cl-2-thiophene	2	0.269 ± 0.017	2.75 ± 0.13	10.2	76.4 ± 5.4	11.5 ± 0.9	6.64
w22	5-Br-2-thiophene	2	0.768 ± 0.037	0.208 ± 0.009	0.271	96.2 ± 4.8	9.47 ± 0.54	10.2
w23	5-CH_3-2-thiophene	2	1.55 ± 0.013	0.370 ± 0.021	0.239	N	N	–
Donepezil	–	–	0.035 ± 0.003	2.32 ± 0.10		nt	nt	–
Galantamine	–	–	2.67 ± 0.18	12.7 ± 0.3		nt	nt	–
Lazabemide	–	–	nt[c]	nt	–	nt	0.105 ± 0.008	–
Iproniazide	–	–	nt	nt	–	6.7 ± 0.4	7.69 ± 0.23	–

[a]IC_{50}: 50% inhibitory concentration (means ± SD of three experiments).
[b]Inactive at 100 μM (highest concentration tested), at higher concentrations the compounds precipitate.
[c]nt = not tested.

Inhibitory activity against MAOs

For all target compounds, the MAO inhibitory activities were measured, and lazabemine and iproniazide were used as reference compounds. The corresponding IC_{50} values and MAO selectivity ratios are also shown in Table 1. Based on the screening data, it could be seen that only a part of the tested compounds could effectively inhibit MAO-A or MAO-B. Among the synthesized compounds, **w20** was the most potent and selective inhibitor against MAO-B (IC_{50} = 2.53 μM, SI > 39.5), which is nearly 3 times stronger than that of iproniazide. Compound **w18** (IC_{50} = 13.4 μM for MAO-A; IC_{50} = 3.14 μM for MAO-B) with 5-Cl substituent at pyridine ring exhibited the most potent MAO-A and MAO-B. From the IC_{50} values, compounds **w1–5** with carboxamide linkage showed no activity, which suggested that the suitable linker length seemed to be 2 carbon atoms for MAOs inhibition.

Compared to no substituted compound **w6** (no activity at 100 μM), introduction of different sizes to the 2-position of phenyl ring also showed no activity at 100 μM with exception of **w8** (IC_{50} = 46.8 μM for MAO-B). Furthermore, among **w6–14**, compounds with 3- and 4-position electron-withdrawing substitutions of phenyl ring were more potent inhibition for MAOs than those with 2-position substitution. Replacement of Cl group (**w18**) with F group (**w19**) in 5-position of pyridine ring presented a total loss of inhibitory activity for both MAO-A and B. In addition, the electronic properties of substitutions at 5-position of thiophene ring also affected the MAOs inhibitory activity. Compared to **w21** and **w22**, compound **w21** (IC_{50} = 76.4 μM for MAO-A; IC_{50} = 11.5 μM for MAO-B, SI = 6.64) and **w22** (IC_{50} = 96 μM for MAO-A; IC_{50} = 9.47 μM for MAO-B, SI = 10.2) were potent for MAO-A and MAO-B, and good selective inhibitors toward MAO-B. Finally, we found that, no matter introducing the Cl group to 4-position of phenyl ring, 5-position of pyridine or thiophene ring, respectively, all of them showed good inhibition for both MAO-A and B.

Inhibitory activity against *h*AChE

Based on the results of ChEs and MAOs inhibitory activity, compounds **w10**, **11**, **14**, **15**, **18**, **21**, **22** showed good inhibition. However, their ChE inhibitory activity was initially tested on enzymes of animal origin due to the lower cost. To better evaluate them, their inhibitory activity was retested on human AChE and the results are summarized in Table 2. Most of the tested compounds gave IC_{50} values in nanomolar, which were slightly less potent inhibition for *h*AChE than for eeAChE. However, compound **w22** exhibited the inhibitory activity for *h*AChE (IC_{50} = 0.363 μM) was 2 times stronger than for eeAChE (IC_{50} = 0.768 μM). Among them, we chose compound **w18**, which showed balanced potential to inhibit ChEs (eeAChE: IC_{50} = 0.220 μM; eqBuChE: IC_{50} = 1.23 μM; hAChE: IC_{50} = 0.454 μM) and MAOs (MAO-A: IC_{50} = 13.4 μM; MAO-B: IC_{50} = 3.14 μM) as a promising multi-targeted inhibitor for further study.

Table 2. Inhibition of human AChE activity.

Compound	R	n	IC_{50}[a] (μM) *h*AChE[b]
w10	3-NO_2 Ph	2	0.544 ± 0.023
w11	4-NO_2 Ph	2	0.325 ± 0.009
w14	4-Cl Ph	2	0.621 ± 0.036
w15	2-quinoline	2	0.527 ± 0.010
w18	5-Cl-2-pyridine	2	0.454 ± 0.023
w21	5-Cl-2-thiophene	2	0.412 ± 0.017
w22	5-Br-2-thiophene	2	0.363 ± 0.027
Donepezil	–	–	0.029 ± 0.002

[a]IC_{50}: 50% inhibitory concentration (means ± SD of three experiments).
[b]AChE from human erythrocytes.

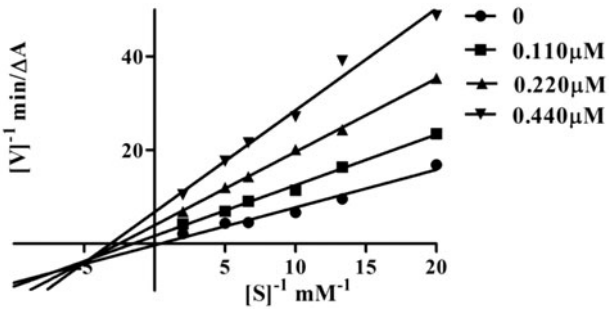

Figure 2. Kinetic study on the mechanism of eeAChE inhibition by compound **w18**. Overlaid Lineweaver–Burk reciprocal plots of AChE initial velocity at increasing substrate concentration (0.05–0.50 mM) in the absence of inhibitor and in the presence of **w18** are shown. Lines were derived from a weighted least-squares analysis of the data points.

Kinetic study of AChE

Kinetic study of compound **w18** was further examined to investigate the AChE inhibitory mechanism. Graphical analysis of the Lineweaver–Burk reciprocal plots (Figure 2) indicated that both increasing slopes and intercepts with increasing inhibitor concentrations. This pattern suggested **w18** is a mixed-type of inhibition and this revealed that it could interact simultaneously with dual sites (PAS and CAS) of AChE. Replots of the slope versus concentration of **w18** gave an estimate of competitive inhibition constant, K_i, of 0.220 μM.

Kinetic study for MAO-B

From the point of view of AD treatment, reversible inhibitors of MAO-B have significant advantages over the irreversible inhibitors. Therefore, to examine whether **w18** was reversible or irreversible MAO-B inhibitor, the time dependencies of inhibition were evaluated with an irreversible inhibitor, pargyline, as reference compound[50]. Compound **w18** was preincubated for various time periods (0–60 min) with human MAO-B at a concentration of 6.28 μM. This concentration of the inhibitor are twofold the measured IC_{50} value for the inhibition of MAO-B. As shown in Figure 3, we could observe that **w18** was reversible MAO-B inhibitors as evidenced by the time-dependent decrease of their inhibitory activity. In contrast, after treatment of MAO-B with pargyline, the enzyme inhibitory activity was increased.

Compound **w18** was also used to further investigate the mode of MAO-B inhibition. The type of MAO-B inhibition was determined by the Michaelis–Menten kinetic experiments[51]. In this study, four different concentrations of **w18** (0, 1.57, 3.14 and 6.28 μM) were selected and five different concentrations of *p*-tyramine (0.05–1 mM) were used as substrate. The overlaid reciprocal Lineweaver–Burk plots (Figure 4) showed that all plots

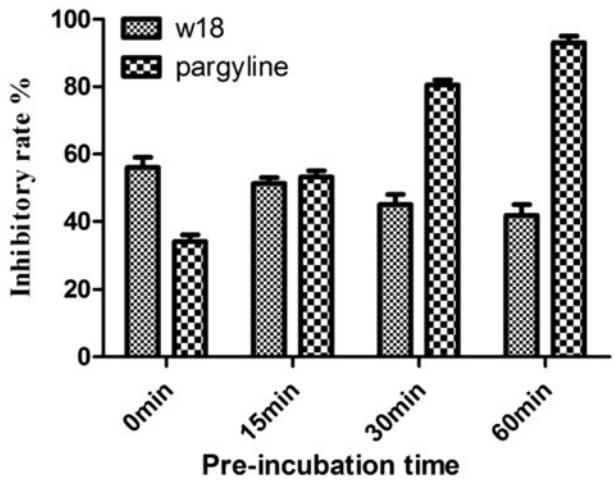

Figure 3. Reversibility studies of hMAO-B inhibition by compound **w18**. Compound **w18** and pargyline were preincubated for various periods of time (0–60 min) with hMAO-B at concentrations equal to twofold the IC_{50} values for the inhibition of the enzyme. After dilution to concentrations of **w18** and pargyline equal to IC_{50}, the inhibitory rates were recorded.

for different concentrations of **w18** were linear and intersected at the *y*-axis. This behavior indicated that compound **w18** acted as a competitive MAO-B inhibitor, and this result further proved that **w18** was reversible MAO-B inhibitor.

Molecular modeling studies of ChEs

To further study the interaction mode of compound **w18** for ChEs, molecular docking study was performed using software package MOE 2008.10. The X-ray crystal structure of the TcAChE complex with donepezil (PDB code: 1EVE) was applied to build the starting model of AChE. As shown in Figure 5(A) and (C), the *N*-benzylpiperidine moiety of **w18** was oriented towards the CAS of AChE, via π-cation interaction with the quaternary nitrogen of piperidine ring from Tyr341 with the distance of 4.26 Å. Besides, its benzene ring could interact with Tyr337 via π–π stacking interaction with the distance of 4.08 Å. The 5-chloropicolinamide moiety interacted with the pridine ring from Trp286 of the PAS via π–π stacking interaction with the distance of 4.35 Å. All these results indicated that compound **w18** was a dual binding site (DBS) AChE inhibitor in agreement with the kinetic study, which demonstrated the rationality of our molecular design.

Since the crystal structure of BuChE from equine serum has not been reported and the sequence of equine BuChE is highly similar to human BuChE, the crystal structure of hBuChE (PDB code: 1P0I) was used in the docking study. As shown in Figure 5(B) and (D), the pyridine ring of **w18** stacked against the Trp82 through a π–π interaction with the distance of 2.76 Å at the CAS.

Molecular modeling studies of MAO-B

To evaluate the binding mode of compound **w18** with MAO-B, docking studies were employed with MOE 2008.10, based on the protein crystal structure of MAO-B (2V60). The 3D and 2D images of binding are illustrated in Figure 6. It can be seen from Figure 6(A) and (B), the *N*-benzylpiperidine moiety of **w18** was located within the substrate cavity of the enzyme, in close proximity of the flavin adenine dinucleotide (FAD) cofactor, and the π–π stacking interaction was seen between its benzene moiety with Tyr398 with the distance of 4.59 Å. Besides, the *N*-benzylpiperidine moiety via π–cation interaction with the quaternary nitrogen of piperidine ring from Gln206 had the distance of

1.75 Å. Finally, the 5-chloropicolinamide moiety of **w18** occupied the hydrophobic pocket in the entrance cavity, formed by Pro104, Ser200, Leu171, Tyr326, Phe103, Pro102, Ile199 and Ile316.

Metal chelating effect

The complexation ability of compound **w18** for Cu^{2+} in methanol was studies by using UV–Vis spectrometry with wavelength ranging from 200 to 500 nm[52,53]. In Figure 7(A), UV–Vis spectra of **w18** at increasing Cu^{2+} concentration were shown. The decrease in absorbance (at about 375 nm peak in Figure 7B), which could be better estimated by an inspection of the differential spectra, indicated that there was an interaction between Cu^{2+} and compound **w18**. These observations indicated that our compounds could effectively chelate Cu^{2+}, and thereby could serve as metal chelators in treating AD.

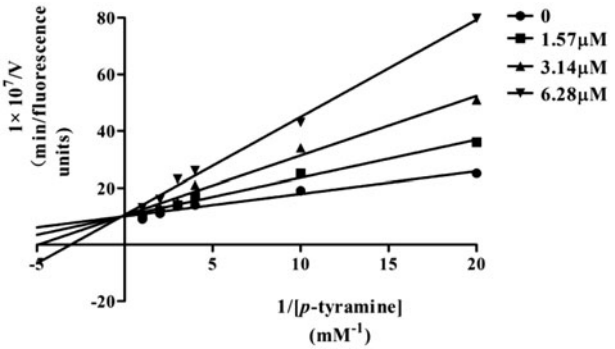

Figure 4. Kinetic study on the mechanism of hMAO-B inhibition by **w18**. Overlaid Lineweaver–Burk reciprocal plots of hMAO-B initial velocity at increasing *p*-tyramine concentration (0.05–1 mM) in the absence of inhibitor and in the presence of **w18** are shown. Lines were derived from a weighted least-squares analysis of the data points.

In vitro BBB permeation assay

Because the first requirement for successful CNS drugs is to reach their therapeutic targets in brain, screening for the BBB penetration is of particular importance[54]. To determine whether the present compounds could penetrate into the brain, we used a parallel artificial membrane permeation assay for BBB (PAMPA-BBB), which was described by Di et al.[55]. Assay validation was performed by comparing experimental permeability of 9 commercial drugs with reported values (Table 3). A plot of experimental data versus bibliographic values gave a good linear correlation, P_e (exp) = 0.85 P_e (bibl.) − 0.13 (R^2 = 0.98). From this equation-and taking into account the limits established by Di et al. for BBB permeation, we established that molecules with permeability values over 3.3×10^{-6} cm s^{-1} would be able to cross the BBB. Three compounds (**w14**, **w18** and **w21**) that exhibited good activities against ChEs and MAOs were chosen as the tested compounds. The results summarized in Table 4 indicated that all of them showed higher P_e values than 3.3, which suggested they were able to cross the BBB and target the enzyme in the central nervous system.

Rat pheochromocytoma (PC12) cell toxicity

The compound **w18** was selected as the candidate to further study the potential toxicity effect on the rat pheochromocytoma (PC12) cells. After incubating the cells to compound **w18** for 24 h, the

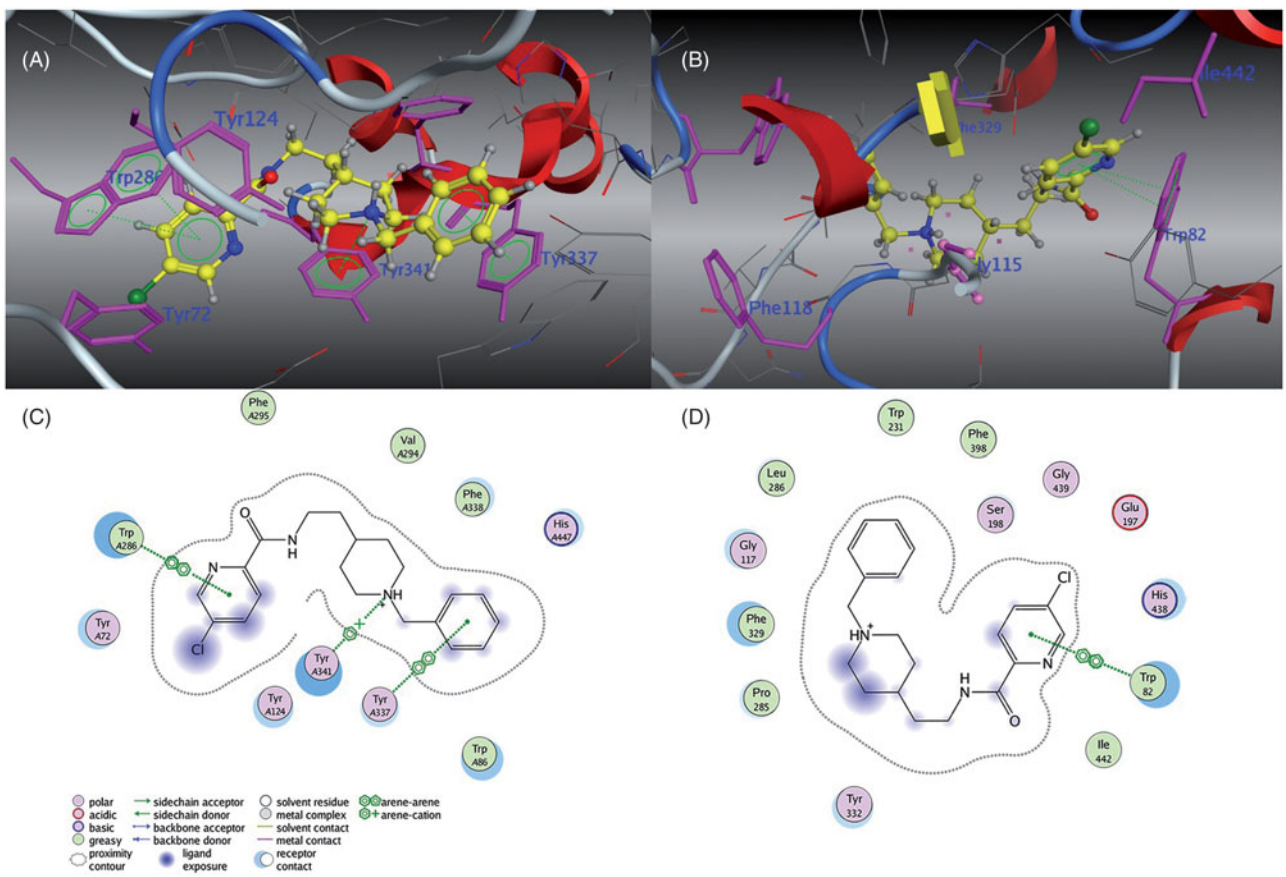

Figure 5. (A) 3D docking model of compound **w18** with TcAChE. (B) 3D docking model of compound **w18** with hBuChE. (C) 2D schematic diagram of docking model of compound **w18** with TcAChE. (D) 2D schematic diagram of docking model of compound **w18** with hBuChE. The figure was prepared using the ligand interactions application in MOE.

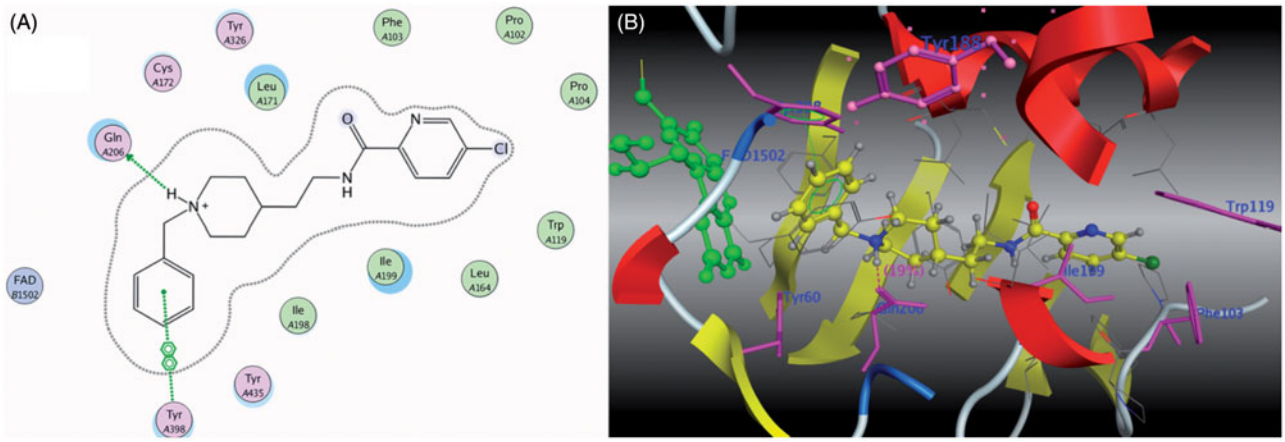

Figure 6. Molecule docking of compound **w18** with hMAO-B generated with MOE: (A) The 2D picture of binding was depicted; (B) The 3D picture of binding was depicted.

Figure 7. (A) UV–Vis (200–500 nm) absorption spectra of compound **w18** (50 μM) in methanol after addition of ascending amounts of $CuCl_2$ (10–80 μM). (B) The differential spectra due to **w18**-Cu^{2+} complex formation obtained by numerical subtraction from the above spectra of those of Cu^{2+} and **w18** at the corresponding concentrations.

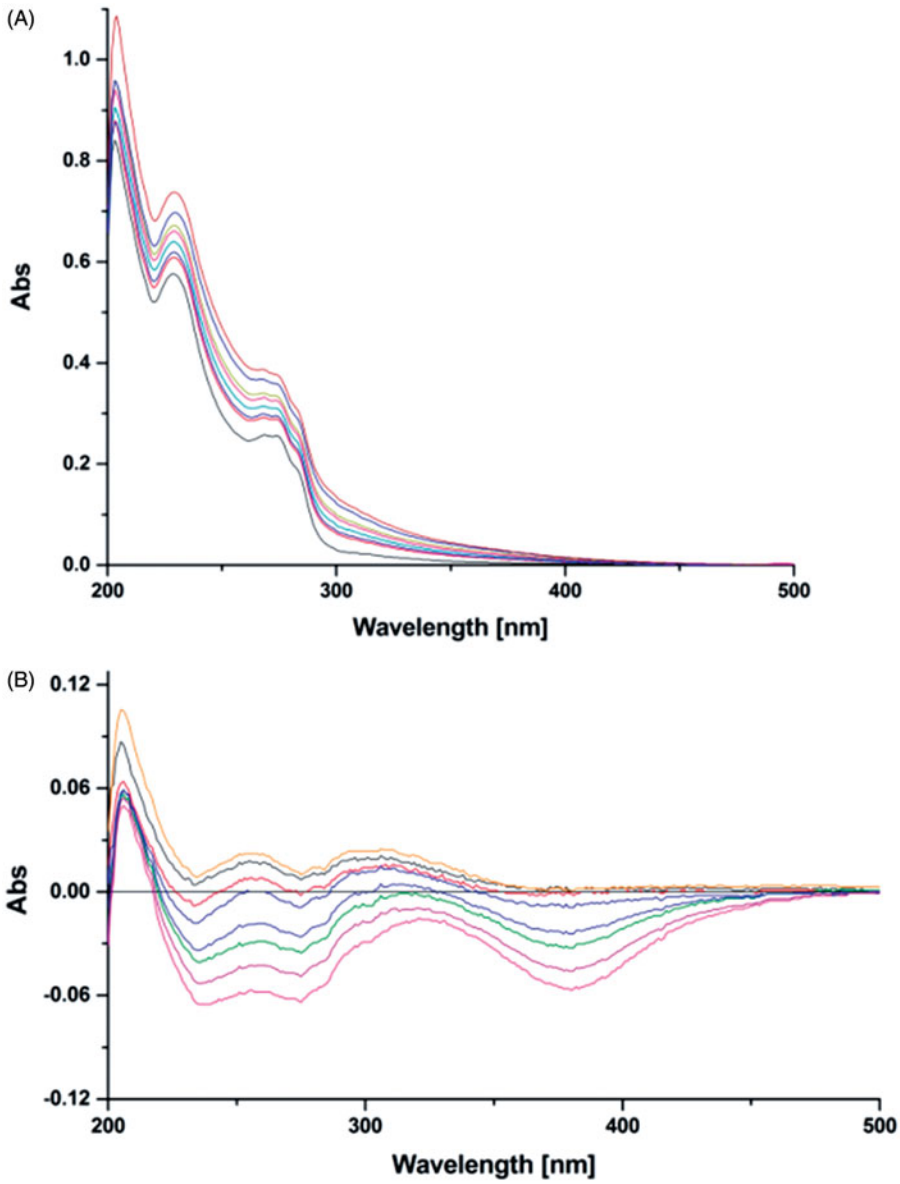

Table 3. Permeability ($P_e \times 10^{-6}$ cm s^{-1}) in the PAMPA-BBB assay for 9 commercial drugs, used in the experiment validation.

Commercial drugs	Bibliography[a]	Experiment[b]
Testosterone	17	15.6 ± 1.03
Verapamil	16	13.2 ± 0.85
β-Estradiol	12	8.90 ± 0.64
Progesterone	9.3	6.62 ± 0.43
Clonidine	5.3	4.74 ± 0.26
Corticosterone	5.1	4.92 ± 0.42
Piroxicam	2.5	1.91 ± 0.17
Hydrocortisone	1.9	1.57 ± 0.12
Dopamine	0.2	0.15 ± 0.01

[a]Taken from Ref[55].
[b]Data are the mean ± SD of three independent experiments.

Table 4. Permeability results ($P_e \times 10^{-6}$ cm s^{-1}) from the PAMPA-BBB assay for selected compounds with their predicted penetration into the CNS.

Compounds	Permeability ($P_e \times 10^{-6}$ cm s^{-1})[a]	Prediction
w14	8.81 ± 1.4	CNS+
w18	10.4 ± 0.9	CNS+
w21	6.57 ± 0.7	CNS+

[a]Data are the mean ± SD of three independent experiments.

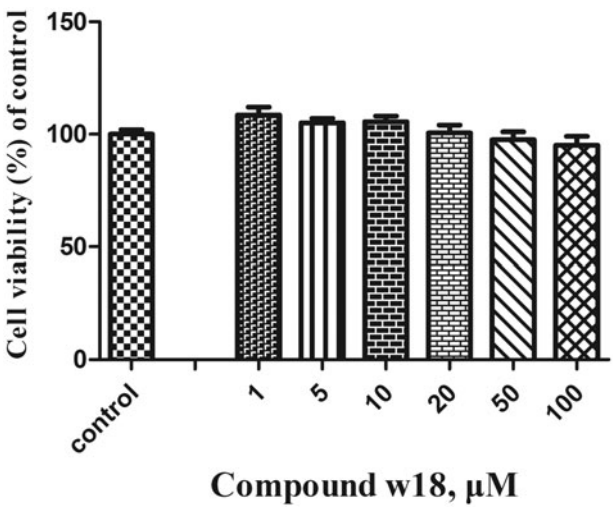

cell viability was tested by the 3-(4,5-dimethylthiazol-2-yl)-2,5-diphenyltetrazolium (MTT) assays. As indicated in Figure 8, **w18** at 1–100 μM did not show significant effect on cell viability. This suggested that compound **w18** was nontoxic to PC12 cells and might be a suitable drug candidate for treating AD.

Conclusion

In summary, a series of donepezil-based compounds have been designed, synthesized and evaluated as multi-functional anti-AD agents with cholinesterase and MAOs inhibitory activities. Most of them displayed potent inhibitory activities toward AChE, BuChE, MAO-B and MAO-A. Among these compounds, some of them may be more potential in some ways, such as **w11**, **w15** were stronger to inhibit ChEs than **w18**, **w20** is more activity to interact with MAOs. But **w18** was the most attractive compound with balanced bioactivity, which is able to inhibit ChEs (eeAChE: $IC_{50} = 0.220\,\mu M$; eqBuChE: $IC_{50} = 1.23\,\mu M$; hAChE: $IC_{50} = 0.454\,\mu M$) and MAOs (MAO-B: $IC_{50} = 3.14\,\mu M$; MAO-A: $IC_{50} = 13.4\,\mu M$). Meanwhile, compound **w18** could penetrate the BBB and showed low cell toxicity on rat pheochromocytoma (PC12) cells *in vitro*. Altogether, the multifunctional ligand **w18** endowed with balanced ChEs and MAOs inhibiting activities might be a promising anti-AD candidate for further research.

Declaration of interest

The authors declare no conflicts of interest.

We gratefully acknowledge the financial support by the National Natural Science Foundation of China (81573313), the program for Changjiang Scholars and Innovative Research Team in University (IRT_15R63), and the Priority Academic Program Development of Jiangsu Higher Education Institutions (PAPD).

References

1. Goedert M, Spillantini MG. A century of Alzheimer's disease. Science 2006;314:777–81.
2. Thies W, Bleiler L. Alzheimer's disease facts and figures. Alzheimer's Dement 2013;9:208–45.
3. Laferla FM, Green KN, Oddo S. Intracellular amyloid-beta in Alzheimer's disease. Nat Rev Neurosci 2007;8:499–509.
4. Bartus RT, Dean RL, Beer B, et al. The cholinergic hypothesis of geriatric memory dysfunction. Science 1982;217:408–14.
5. Xie Q, Wang H, Xia Z, et al. Bis-(-)-nor-meptazinols as novel nanomolar cholinesterase inhibitors with high inhibitory potency on amyloid-beta aggregation. J Med Chem 2008;51:2027–36.
6. Munoz-Torrero D. Acetylcholinesterase inhibitors as disease-modifying therapies for Alzheimers disease. Curr Med Chem 2008;15:2433–55.
7. Greig NH, Utsuki T, Yu Q-S, et al. A new therapeutic target in Alzheimer's disease treatment: attention to butyrylcholinesterase. Curr Med Res Opin 2001;17:159–65.
8. Luo W, Li Y-P, He Y, et al. Design, synthesis and evaluation of novel tacrine-multialkoxybenzene hybrids as dual inhibitors for cholinesterases and amyloid beta aggregation. Bioorg Med Chem 2011;19:763–70.
9. Mesulam MM, Guillozet A, Shaw P, et al. Acetylcholinesterase knockouts establish central cholinergic pathways and can use butyrylcholinesterase to hydrolyze acetylcholine. Neuroscience 2002;110:627–39.
10. Fernández-Bachiller MI, Pérez C, Monjas L, et al. New tacrine-4-oxo-4H-chromene hybrids as multifunctional agents for the treatment of Alzheimer's disease, with cholinergic, antioxidant, and β-amyloid-reducing properties. J Med Chem 2012;55:1303–17.
11. Perry EK, Perry RH, Blessed G, et al. Changes in brain cholinesterases in senile dementia of Alzheimer type. Neuropathol Appl Neurobiol 1978;4:273–7.
12. Shih JC, Chen K, Ridd MJ. Monoamine oxidase: from genes to behavior. Annu Rev Neurosci 1999;22:197–217.
13. Mellick GD, Buchanan DD, Mccann SJ, et al. Variations in the monoamine oxidase B (MAOB) gene are associated with Parkinson's disease. Mov Disord 1999;14:219–24.
14. Bach A, Lan NC, Johnson DL, et al. cDNA cloning of human liver monoamine oxidase A and B: molecular basis of differences in enzymatic properties. Proc Natl Acad Sci USA 1988;85:4934–8.
15. Wouters J. Structural aspects of monoamine oxidase and its reversible inhibition. Curr Med Chem 1998;5:137.
16. Edmondson DE, Binda C, Wang J, et al. Molecular and mechanistic properties of the membrane-bound mitochondrial monoamine oxidases. Biochemistry 2009;48:4220–30.
17. Tipton KF, Boyce S, O'sullivan J, et al. Monoamine oxidases: certainties and uncertainties. Curr Med Chem 2004;11:1965–82.
18. Chen JJ, Swope DM, Dashtipour K. Comprehensive review of rasagiline, a second-generation monoamine oxidase inhibitor, for the treatment of Parkinson's disease. Clin Ther 2007;29:1825–49.

19. Nebbioso M, Pascarella A, Cavallotti C, et al. Monoamine oxidase enzymes and oxidative stress in the rat optic nerve: age-related changes. Int J Exp Pathol 2012;93:401–5.
20. Weyler W, Hsu Y-PP, Breakafield XO. Biochemistry and genetics of monoamine oxidase. Pharmacol Ther 1990;47:391–417.
21. Chen Y, Sun J, Fang L, et al. Tacrine-ferulic acid-nitric oxide (NO) donor trihybrids as potent, multifunctional acetyl- and butyrylcholinesterase inhibitors. J Med Chem 2012;55:4309–21.
22. Tomassoli I, Ismaili L, Pudlo M, et al. Synthesis, biological assessment and molecular modeling of new dihydroquinoline-3-carboxamides and dihydroquinoline-3-carbohydrazide derivatives as cholinesterase inhibitors, and Ca channel antagonists. Eur J Med Chem 2011;46:1–10.
23. Morphy R, Rankovic Z. Designed multiple ligands. An emerging drug discovery paradigm. J Med Chem 2005;48:6523–43.
24. Zemek F, Drtinova L, Nepovimova E, et al. Outcomes of Alzheimer's disease therapy with acetylcholinesterase inhibitors and memantine. Expert Opin Drug Saf 2014;13:759–74.
25. León R, Garcia AG, Marco-Contelles J. Recent advances in the multitarget-directed ligands approach for the treatment of Alzheimer's disease. Med Res Rev 2013;33:139–89.
26. Fink DM, Palermo MG, Bores GM, et al. Imino 1,2,3,4-tetrahydrocyclopent[b]indole carbamates as dual inhibitors of acetylcholinesterase and monoamine oxidase. Bioorg Med Chem Lett 1996;6:625–30.
27. Sterling J, Herzig Y, Goren T, et al. Novel dual inhibitors of AChE and MAO derived from hydroxy aminoindan and phenethylamine as potential treatment for Alzheimer's disease. J Med Chem 2002;45:5260–79.
28. Xie S-S, Wang X-B, Li J-Y, et al. Design, synthesis and evaluation of novel tacrine–coumarin hybrids as multifunctional cholinesterase inhibitors against Alzheimer's disease. Eur J Med Chem 2013;64:540–53.
29. Hamulakova S, Janovec L, Hrabinova M, et al. Synthesis and biological evaluation of novel tacrine derivatives and tacrine-coumarin hybrids as cholinesterase inhibitors. J Med Chem 2014;57:7073–84.
30. Cheung J, Rudolph MJ, Burshteyn F, et al. Structures of human acetylcholinesterase in complex with pharmacologically important ligands. J Med Chem 2012;55:10282–6.
31. Korabecny J, Dolezal R, Cabelova P, et al. 7-MEOTA-donepezil like compounds as cholinesterase inhibitors: synthesis, pharmacological evaluation, molecular modeling and QSAR studies. Eur J Med Chem 2014;82:426–38.
32. Bolea I, Juárez-Jiménez J, de los Ríos CB, et al. Synthesis, biological evaluation, and molecular modeling of donepezil and *N*-[(5-(benzyloxy)-1-methyl-1 *H*-indol-2-yl)methyl]-*N*-methylprop-2-yn-1-amine hybrids as new multipotent cholinesterase/monoamine oxidase inhibitors for the treatment of Alzheimer's disease. J Med Chem 2011;54:8251–70.
33. Da Prada M, Kettler R, Keller HH, et al. Neurochemical profile of moclobemide, a short-acting and reversible inhibitor of monoamine oxidase type A. J Pharmacol Exp Ther 1989;248:400–14.
34. Haefely W, Kettler R, Keller H, et al. Ro 19-6327, a reversible and highly selective monoamine, oxidase B inhibitor: a novel tool to explore the MAO-B function in humans. Adv Neurol 1990;53:505.
35. Carlsson M, Carlsson A. Interactions between glutamatergic and monoaminergic systems within the basal ganglia-implications for schizophrenia and Parkinson's disease. Trends Neurosci 1990;13:272–6.
36. Miura H, Naoi M, Nakahara D, et al. Effects of moclobemide on forced-swimming stress and brain monoamine levels in mice. Pharmacol Biochem Behav 1996;53:469–75.
37. Haefely W, Burkard WP, Cesura AM, et al. Biochemistry and pharmacology of moclobemide, a prototype rima. Psychopharmacology (Berlin) 1992;106:6–14.
38. Sun Y, Chen J, Chen X, et al. Inhibition of cholinesterase and monoamine oxidase-b activity by Tacrine-Homoisoflavonoid hybrids. Bioorg Med Chem 2013;21:7406–17.
39. Bautista-Aguilera OM, Esteban G, Chioua M, et al. Multipotent cholinesterase/monoamine oxidase inhibitors for the treatment of Alzheimer's disease: design, synthesis, biochemical evaluation, ADMET, molecular modeling, and QSAR analysis of novel donepezil-pyridyl hybrids. Drug Des Devel Ther 2014;8:1893–10.
40. Mao F, Chen J, Zhou Q, et al. Novel tacrine–ebselen hybrids with improved cholinesterase inhibitory, hydrogen peroxide and peroxynitrite scavenging activity. Bioorg Med Chem Lett 2013;23:6737–42.
41. Golbraikh A, Bernard P, Chrétien JR. Validation of protein-based alignment in 3D quantitative structure-activity relationships with CoMFA models. Eur J Med Chem 2000;35:123–36.
42. Tong W, Collantes ER, Chen Y, et al. A comparative molecular field analysis study of N-benzylpiperidines as acetylcholinesterase inhibitors. J Med Chem 1996;39:380–7.
43. Manetti D, Martini E, Ghelardini C, et al. 4-Aminopiperidine derivatives as a new class of potent cognition enhancing drugs. Bioorg Med Chem Lett 2003;13:2303–6.
44. López-Iglesias B, Pérez C, Morales-García JA, et al. New melatonin-N, N-dibenzyl(N-methyl)amine hybrids: potent neurogenic agents with antioxidant, cholinergic, and neuroprotective properties as innovative drugs for Alzheimer's disease. J Med Chem 2014;57:3773–85.
45. Ehret F, Bubrin M, Záliš S, et al. Metal-chelating N,N′-Bis(4-dimethylaminophenyl)acetamidinyl radical: a new chromophore for the near-infrared region . Chemistry 2015;21:12275–8.
46. Li S-Y, Jiang N, Xie S-S, et al. Design, synthesis and evaluation of novel tacrine-rhein hybrids as multifunctional agents for the treatment of Alzheimer's disease. Org Biomol Chem 2014;12:801–14.
47. Sugimoto H, Tsuchiya Y, Sugumi H, et al. Novel piperidine derivatives. Synthesis and anti-acetylcholinesterase activity of 1-benzyl-4-[2-(n-benzoylamino)ethyl]piperidine derivatives. J Med Chem 1990;33:1880–7.
48. Prieto J, Moragues J, Spickett R, et al. Synthesis and pharmacological properties of a series of antidopaminergic piperidyl benzamides. J Pharm Pharmacol 1977;29:147–52.
49. Ellman GL, Courtney KD, Andres V, et al. A new and rapid colorimetric determination of acetylcholinesterase activity. Biochem Pharmacol 1961;7:88–95.
50. Legoabe LJ, Petzer A, Petzer JP. Selected c7-substituted chromone derivatives as monoamine oxidase inhibitors. Bioorg Chem 2012;45:1–11.
51. Pérez V, Marco JL, Fernández-lvarez E, et al. Relevance of benzyloxy group in 2-indolyl methylamines in the selective MAO-B inhibition. Br J Pharmacol 1999;127:869–76.
52. Bolognesi ML, Cavalli A, Valgimigli L, et al. Multi-target-directed drug design strategy: from a dual binding site acetylcholinesterase inhibitor to a trifunctional compound against Alzheimer's disease. J Med Chem 2007;50:6446–9.
53. Huang W, Lv D, Yu H, et al. Dual-target-directed 1,3-diphenylurea derivatives: Bace 1 inhibitor and metal chelator against Alzheimer's disease. Bioorg Med Chem 2010;18:5610–15.
54. Pardridge WM. Alzheimer's disease drug development and the problem of the blood–brain barrier. Alzheimers Dement 2009;5:427–32.
55. Di L, Kerns EH, Fan K, et al. High throughput artificial membrane permeability assay for blood–brain barrier. Eur J Med Chem 2003;38:223–32.

Supplementary material available online